Review Article **Open Access**

Talha Erdem and Hilmi Volkan Demir*

Colloidal nanocrystals for quality lighting and displays: milestones and recent developments

DOI 10.1515/nanoph-2016-0009
Received October 1, 2015; accepted October 1, 2015

Abstract: Recent advances in colloidal synthesis of nanocrystals have enabled high-quality high-efficiency light-emitting diodes, displays with significantly broader color gamut, and optically-pumped lasers spanning the whole visible regime. Here we review these colloidal platforms covering the milestone studies together with recent developments. In the review, we focus on the devices made of colloidal quantum dots (nanocrystals), colloidal quantum rods (nanorods), and colloidal quantum wells (nanoplatelets) as well as those of solution processed perovskites and phosphor nanocrystals. The review starts with an introduction to colloidal nanocrystal photonics emphasizing the importance of colloidal materials for light-emitting devices. Subsequently, we continue with the summary of important reports on light-emitting diodes, in which colloids are used as the color converters and then as the emissive layers in electroluminescent devices. Also, we review the developments in color enrichment and electroluminescent displays. Next, we present a summary of important reports on the lasing of colloidal semiconductors. Finally, we summarize and conclude the review presenting a future outlook.

Talha Erdem: Department of Electrical and Electronics Engineering, Department of Physics, Institute of Materials Science and Nanotechnology, and UNAM-National Nanotechnology Research Center, Bilkent, Ankara Turkey 06800
***Corresponding Author: Hilmi Volkan Demir:** Department of Electrical and Electronics Engineering, Department of Physics, Institute of Materials Science and Nanotechnology, and UNAM-National Nanotechnology Research Center, Bilkent, Ankara Turkey 06800 and Luminous! Center of Excellence for Semiconductor Lighting and Displays, School of Electrical and Electronic Engineering, School of Physical and Mathematical Sciences, School of Materials Science and Engineering, Nanyang Technological University, Singapore 639798, E-mail: volkan@bilkent.edu.tr

1 Introduction

Since the end of the 20th century, we have been witnessing the advance of electronics and photonics in a mutual relation. The developments in one field clearly contribute to further developments in the other. An important binding force of this relation has been the research on emerging materials including in all disciplines of materials science, chemistry, physics, and electrical engineering. Thanks to these multidisciplinary efforts at a global scale, today we have very sophisticated optoelectronic devices, for example, luminaries, displays, sensors, imaging tools, etc. Especially within the last two decades, significant contributions to photonics have come from the science and technology of semiconductor colloids [1–6] leading to today's commercial devices [7, 8] made of colloidal semiconductor nanoparticles. Some of the attractive features of these colloidal materials can be listed as their high quantum efficiencies, precisely controllable emission colors, narrow emission bandwidths, large absorption cross sections, improved stabilities, cost-effectiveness, and abundance [9]. Among the devices involving colloidal materials, in this review we focus on the light-emitting devices, in particular, light-emitting diodes (LEDs), displays, and lasers in which colloidal semiconductor quantum dots (QDs), rods (also known as nanorods), and wells (also known as nanoplatelets, NPLs) along with perovskites and phosphor nanocrystals are utilized. Here, we summarize early milestone works and recent important advancements on these topics for each device.

LEDs were one of the first devices utilizing colloidal semiconductor nanoparticles, which offer spectral tuning in white light generation along with high efficiencies and high quality lighting for indoor [10] and outdoor [11] lighting applications. In LEDs, colloidal nanoparticles were employed as both color converters typically on epitaxially grown LEDs and as emissive layers of electroluminescent devices. In the LEDs employing colloidal nanoparticles as color converters, the color-conversion layer is, in general, prepared by blending the colloidal material within a polymeric encapsulation matrix and placed on

top of a near-ultraviolet (near-UV) or blue-emitting LED chip that subsequently excites the colloidal semiconductors in the film. In the electroluminescent devices, the colloidal materials were usually sandwiched between layers of hole injection and transport, and layers of electron injection and transport. Electroluminescence is obtained through the radiative recombination of injected electrons and holes within the colloidal semiconductor material. A major advantage of using colloidal materials in both color-converting and electroluminescent LEDs comes from their narrow-band emission spectra allowing for quality white-light-emitting devices. As a result, high color rendition performance along with high photometric efficiency can be realized at the same time [12]. In addition, due to the rising concerns regarding the supply of rare-earth ion based phosphors [13], colloidal semiconductor materials have stepped forward in recent years [14] since they can be synthesized from abundant materials having supply chains more immune to political tensions.

Similar to lighting, colloidal materials have been investigated in displays as color converters and also as active electroluminescence layers. Their use in displays for lighting inherits significant similarities; however, the use of colloidal materials in displays poses additional advantages. First of all, purer colors (in other words, more saturated colors in color science terms) can be realized as a result of significantly narrow band edge emission of the colloidal materials. These pure colors obtained from colloids increase the range of colors that can be defined by the display [15], which is also known as the color gamut. When these materials are utilized as color converters, they are in general integrated on a blue LED chip as in the case of lighting applications or as a remote color converter in a glass tube on the periphery of the optical back plane or in a plastic film on the back plane of the display away from LEDs. The generated light then passes through polarizers, color filters, and liquid crystals to obtain the desired color controlled at individual pixel level [16]. The use of the colloidal materials as active emissive layers in electroluminescent devices, on the other hand, requires pixelated formation of the LEDs. In these displays, there is no need to use color filters or polarizers, which block a significant amount of light leading to decreased efficiencies and heating, if single colored LEDs controlled at individual pixel levels are employed.

The application of the colloidal materials in lasers has also attracted significant attention because these materials enable color control of the laser by size and composition tuning of the colloidal material. Furthermore, significant cost reductions compared with conventional methods can be realized if electroluminescent solid-state lasers of colloids can be developed. However, in contrast to LEDs and displays, the problems that need to be overcome to realize colloidal lasers are more serious. Since the lasers operate in the nonlinear regime in which the population inversion of electrons and holes is required, suppression of all the loss mechanisms including Auger recombination and surface traps and increasing the stability of the emitters are of significant importance [17]. Therefore, developing lasers involving colloidal emitters takes more effort but it is also an open field for further improvements. To date, no electrically driven laser of colloidal materials could be presented; however, a wide variety of lasers with optical excitation have already been reported for QDs, nanorods, NPLs, and perovskites.

2 Color-converting colloidal materials for lighting

High-quality lighting requires the optimization of various performance metrics including the ability to render the real colors of the objects along with a strong overlap of the emission spectrum with the eye sensitivity function and a warm white shade [15]. The color rendition capability of the light sources is, in general, evaluated using color rendering index (CRI). The worst color rendition performance is quantified with −100 while the perfect performance is 100. In addition to the color rendition performance of the light source, it is also important to maximize the fraction of the light produced by the light source that can be perceived by the human eye. Even if the emitter is quantum mechanically very efficient, it might not have any meaning as a light source for general lighting applications in the case that the optical power is wasted in the spectral regime where the human eye is not sensitive. Therefore, overlap of the emission spectrum with the human eye sensitivity function is very crucial for efficient illumination. This overlap is quantified using luminous efficiency (LE) of the optical radiation (LER), which takes values >350 $\mathrm{lm/W}_{opt}$ for high-efficiency light sources. The electrical efficiency of the light source is also an important parameter for the performance of a light source. This metric is typically evaluated using the LE (sometimes also referred to as power efficiency), which is basically the product of LER and the power conversion efficiency. Current phosphor based LEDs reach LEs >140 $\mathrm{lm/W}_{elect}$ [18] while reaching an LE of 100 $\mathrm{lm/W}_{elect}$ is still a challenge for colloidal material integrated white LEDs. Another important parameter in the white light source design is its shade. In general, a warm white shade is preferable over a cool white

light for indoor use. This feature of the light source is evaluated using correlated color temperature (CCT). A warm white light source has a CCT below 4500 K while a cool white light source has higher CCTs. For detailed information on these metrics and their simultaneous optimization the reader can refer to a previous review on the color science of colloidal semiconductors [15].

The optimization of all these metrics at the same time is not trivial and needs careful control of the light source spectrum. Colloidal materials having narrow band emission such as semiconductor QDs, NPLs, and perovskites help to solve this problem since they allow for spectral tuning. Within this framework, we studied the necessary conditions for high photometric efficiency lighting using QD color converters on LEDs [12] and found that the red color component is especially important. The peak emission wavelength of this color component should be at 620 nm, its full width at half-maximum should be as narrow as possible (ideally <30 nm), and it should be the most dominant color component of the LED spectrum. On the other hand, the blue color component should be the weakest component in the emission spectrum. Based on these theoretical findings we carried out an experimental demonstration of a high-quality QD integrated white LED [10]. In this work, CdSe/ZnS QDs embedded into poly(methyl methacrylate) (PMMA) were employed as color converters on blue LED chips. By carefully controlling the QD amount, we optimized the photometric performance and obtained a CRI ~90 and LER >350 lm/W_{opt} at a CCT <3000 K (Fig. 1(a), also see Table 1 for a summary of the LED performances covered in this review).

Later in 2011 Kim et al. addressed the degradation problem of the QD intensity when embedded within a polymer matrix [19]. This is an important problem for efficient light sources because decreasing quantum efficiencies of the QDs directly affect the LE of the LED since different QDs age at different rates; this constitutes a difficult problem for maintaining the operating point of the LED over time in terms of its photometric figure of merits. These authors also proposed UV irradiation of the QDs in a thermally curable polymer mixture following thermal treatment. It was observed that the emission intensities of the core/shell QDs and core/multishell QDs increase to 230% and 180% of the initial level, respectively. To identify the underlying effect, the transmission electron microscopy images of the hybrid films before and after UV treatment were taken. The images show that UV treatment helps the QDs to be distributed uniformly inside the film while the QDs were rather randomly distributed prior to UV irradiation (Fig. 1(b)). In addition, the authors state that UV treatment allows for better surface passivation of the QDs leading to higher quantum efficiencies. Based on these findings, the authors blended red-emitting QDs with green-yellow phosphors inside the same polymer matrix. Following the UV treatment, a significant improvement in the red color content of the LED was observed and CRI of the white LED increased from 87.2 to 91.0. In 2014 Liang et al. developed controllable incorporation of the QDs into poly(vinyl alcohol) (PVA) matrix to obtain flexible color converters [20]. In this work, single color QDs (green, yellow, orange, and red) were blended within PVA solution to obtain negatively charged QD cluster suspensions. Subsequently, these QDs were assembled in a layer-by-layer fashion on a polyethylene terephthalate substrate using MgAl-NO_3 layered double hydroxides. The quantum efficiencies of these films were ~70% of their initial efficiencies. Green-emitting and red-emitting films were placed on a blue LED chip to realize a white LED, which exhibited a CRI of 92 at a correlated color temperature of 3442 K.

Another important design parameter for high-efficiency QD-white LEDs is the way that the QDs are assembled on the blue LEDs. In this previous work, we computationally showed that blending the QDs of different colors and forming their films cause inefficient performance [21]. These calculations revealed that the best performance can be obtained if the QDs are carefully assembled on a blue LED in a way that the red-emitting QDs remain on the bottom and the green-emitting QDs constitute the top layer. Assembling the QDs in the reversed order (or blending them, for the same matter) is found to decrease the overall efficiency of the film due to self-absorption effect. Based on this idea, Zhao et al. fabricated a QD-integrated white LED and demonstrated that blending the QDs exhibited 30% less LE compared with the layered architecture (Fig. 1(c)) [22]. Another solution to the reabsorption problem is the utilization of doped QDs in which the dopant emission can only be obtained through the excitation of the high-energy band gap host QD. In these materials, the dopant emission cannot be reabsorbed by the QD itself, therefore, the self-absorption effects are significantly reduced. Recently, Zhang et al. have used this idea to fabricate a white QD-integrated LED using Cu doped CdS/ZnSe core/shell QDs in which Cu is doped in the CdS core [23]. This LED reached a CRI of 92 at a CCT of 5854 K. A similar methodology was followed by Xuan et al. to fabricate white LEDs [24]. In this work, the researchers doped the ZnS shell of the CdS/ZnS core/shell QD and employed these QDs as color converters together with a green-yellow phosphor on white LEDs. This LED exhibited an LE of 46.5 lm/W_{elect}, a CRI of 90, and a CCT of 6591 K.

It is a well known fact that the QD emission intensity weakens [25] when strong optical excitation is applied due to issues related to photostability or when the QDs are subjected to high temperatures due to thermal droop, which is the case for the QDs integrated on high-power LEDs. To address this problem, researchers from Samsung proposed the integration of QDs into silica monoliths [26]. Prior to this cited work, the Stöber method has been successfully applied to semiconductor nanoparticles [27]; however, the decrease in the quantum efficiencies was inevitable [26]. Instead of the Stöber method, Jun et al. suggested homogenous doping of QDs into silica monoliths (Fig. 1(d)), which was shown to protect the initial quantum efficiency of the QDs. These silica monoliths, whose external quantum efficiencies (EQEs) were recorded at 89%, were then integrated on to a blue LED. The stability of the silica monoliths was tested on a near-UV LED under high current operation. The QDs within silica monoliths maintained their initial intensity for a long time (>150 h) while the QDs in silicone film significantly degraded. With the same motivation, Yoo et al. uniformly incorporated QDs into 100 nm sized silica nanoparticles [28]. The QD-to-QD distance in these nanoparticles was longer than 14 nm, which weakens the nonradiative energy transfer between the QDs by avoiding excitonic sink in the defected QD subpopulation and keeps the overall quantum efficiency at a higher level. Furthermore, the phenylethyl groups attached to silica nanoparticles that are compatible with the silicone encapsulants resulted in improved light extraction from their white LEDs. A proof-of-concept white QD-LED was prepared by hybridizing these QDs with a yellow-emitting phosphor. The final device exhibited an LE of 58.2 lm/W_{elect} and a CRI of 81.8 while the original QD-integrated LED had an LE of 39.6 lm/W_{elect} and a CRI of 78.1. In addition, the stability of the LED with QDs in the silica nanoparticles retained 95% of the initial intensity while the LED with original QDs kept 91% of its original intensity.

In 2012, Otto et al. addressed this stability problem with a simple but innovative approach [29]. In this work, the researchers incorporated aqueous QDs into ionic salts such as NaCl and KCl simply by slowly evaporating the water of the salt solution-QD dispersion mixture. At the end of the crystallization process, the authors obtained cm-sized macrocrystals of QDs (Fig. 1(e)) with significantly improved photostability compared with bare QDs. A proof-of-concept white LED was subsequently prepared. Kalytchuk et al. applied the same idea to CdTe QDs by using NaCl as the host matrix and prepared single-color LEDs spanning the whole visible regime [33]. They showed that the quantum efficiency of the CdTe QDs improves after incorporation into salt matrix. Later, Müller et al. showed that the quantum efficiency of the QDs in the salt macrocrystals is strongly dependent on the crystallization speed [34] and it can exceed that of the QDs in dispersion if the salt crystallization is slow enough. Another recent work reported the co-immobilization of gold nanoparticles and CdTe QDs in sucrose crystals (Fig. 1(f)) and showed efficiency enhancement of the QDs (by 58%) via plasmonic interaction [30]. However, all these demonstrations of QD macrocrystals required the utilization of aqueous QDs. This, therefore, necessitated a ligand exchange procedure if high-efficiency nonpolar QDs were to be utilized. Nonetheless, it is well known that such a ligand exchange procedure can significantly decrease the efficiency of the QDs. Our group addressed this issue by specifically employing LiCl as the host matrix [35], which can be dissolved in tetrahydrofuran. Since the nonpolar QDs can also be dispersed in tetrahydrofuran, incorporation of the nonpolar QDs into LiCl has been possible without ligand exchange. We showed that this encapsulation technique protects the quantum efficiencies of QDs. Furthermore, when these LiCl-encapsulated QDs were integrated on an LED under high current operation, the intensity of the QDs decreased by only less than 5% while the intensity of the same QDs without LiCl incorporation decreased by about 65% after 4 days of operation at high currents.

Despite their high efficiencies and narrow-band emission, Cd-containing QDs suffer from their recycling difficulties and cost. This problem is typically confused with toxicity. In these QDs, Cd is in its compound form. Unless the particle is not charged, there are examples in the literature showing biocompatible Cd-containing nanocrystals [36]. Currently, for ecofriendliness, there is a huge demand for developing alternative Cd-free QDs having high efficiencies [15]. At this point, Cu and In based QDs step forward. In recent years, these QDs have been successfully implemented in QD-LEDs and significant performance improvements were observed. For example, in 2013 Chen et al. hybridized red-emitting $CuInS_2$ QDs with YAG:Ce phosphor and used this film as a color converter on a blue LED [37]. When no QD was employed, the white LED had an LE of 106.9 lm/W_{elect} and a CRI of 71.2 at a CCT of 5423 K. Hybridization of the phosphor with QD, on the other hand, increased the CRI to 81.9 without any major change in the CCT. However, the LE of the white LED decreased to 91.4 lm/W_{elect}. This decrease emanates from the lower quantum efficiency of the QDs compared with phosphors and also from the tail of QD emission toward longer wavelengths where human eye is not sensitive. On the other hand, strengthened red content in the emission spectrum contributed to an improved CRI. The

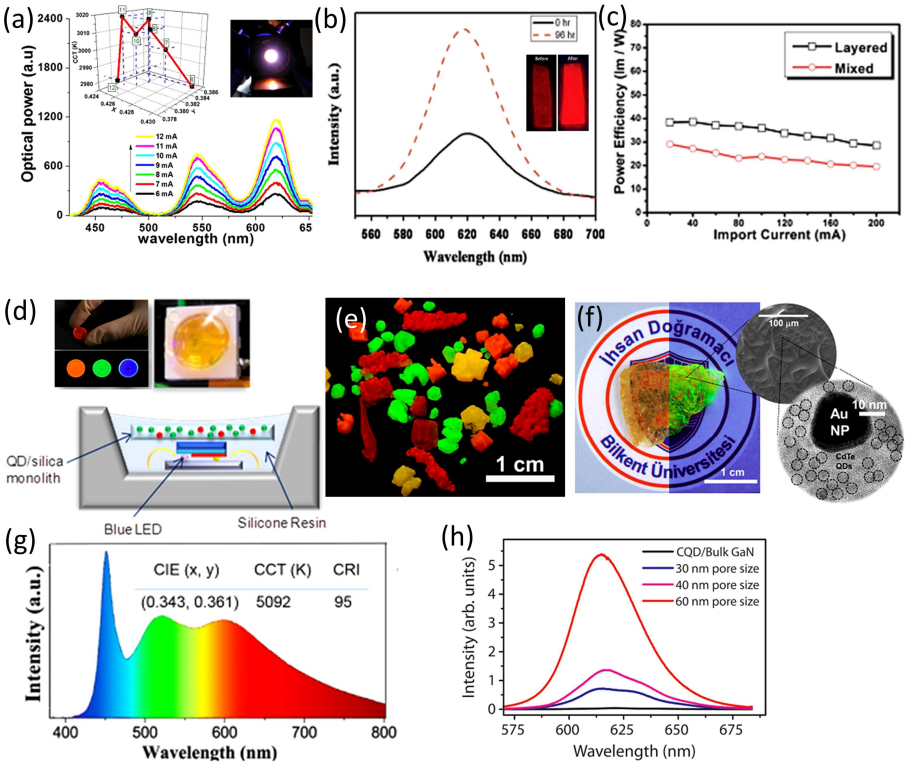

Figure 1: (a) Spectrum of the quantum dot (QD)-integrated white light-emitting diode (LED) exhibiting a color rendering index (CRI) ~90, luminous efficiency of the optical radiation (LER) = 357 lm/W_{opt}, and correlated color temperature (CCT) = 2982 K. Reproduced with permission from Ref. [10], Copyright Optical Society of America. (b) Photoluminescence of the red-emitting QDs embedded within silicone before (black curve) and after (red curve) ultraviolet (UV) treatment along with the real-color photographs of their films under UV illumination before and after the UV treatment (inset). Reproduced with permission from Ref. [19], Copyright Wiley International. (c) Luminous efficiency (also known as power efficiency) of the white LEDs produced by applying layered QD architecture (black) and mixed QD architecture (red) on a blue LED. Reproduced with permission from Ref. [22], Copyright Royal Society of Chemistry. (d) Illustration of the white LED produced using silica monolith along with the single color QD incorporated silica monoliths and the real-color photograph of the white LED. Reproduced with permission from Ref. 26, Copyright American Chemical Society. (e) Real-color photographs of the QD-embedded salt macrocrystals under UV illumination. Reproduced with permission from Ref. [29], Copyright American Chemical Society. (f) Real color- photograph of QD and Au NP co-immobilized macrocrystals exhibiting fluorescence enhancement under ambient lighting and UV illumination along with their scanning electron microscopy and transmission electron microscopy images. Reproduced with permission from Ref. [30], Copyright Tsinghua University Press and Springer-Verlag Berlin. (g) Emission spectrum of the Cu and Mn-doped QD integrated white LED. Reproduced with permission from Ref. [31], Copyright American Chemical Society. (h) Emission spectrum of the red-emitting QDs placed on bulk and porous GaN surface with varying pore sizes. Reproduced with permission from Ref. [32], Copyright Wiley International.

same group also reported another color-converting LED of $CuInS_2$/ZnS QDs spanning the visible regime. Employing green-emitting and red-emitting QDs together with a blue LED, they obtained an LE of 69.4 lm/W_{elect}, a CRI of 95.1, and a CCT of 5322 K [38]. In 2014 Kim et al. reported the white LED prepared using free-standing films of green-emitting hydrophilic $CuIn_{0.2}Ga_{0.8}S$/ZnS QDs embedded into PVA and red-emitting hydrophobic InP/ZnS QDs embedded into poly(vinyl pyrolidone) [39]. The resulting white LED had a CRI of 94 and a CCT of 5322 K with an LE of 34.2 lm/W_{elect}. In 2015 Yoon et al. reported a green-emitting Zn-Ag-In-S and red-emitting Zn-Cu-In-S QD incorporated white LED [40]. This LED exhibited an extraordinary level of CRI performance by achieving values >95 with a LE of 54 lm/W_{elect} at a CCT of 6500 K. In these LEDs, the self-absorption problem was unavoidable because the QDs having broad emissions absorb their own photons, which eventually contributes to reduced quantum efficiencies. As a remedy to this problem, doping the QDs with metal ions can be helpful because the long-wavelength emission associated with the dopants cannot be absorbed by the QDs themselves. Within this approach, Huang et al. synthesized Mn-doped $CuInS_2$/ZnS QDs [41]. In these QDs, Mn ions were doped in the shell of the QDs so that two-color emission can be observed from the same QD. The green emission of these QDs was associated with Mn dopants in

the shell while the reddish emission came from the $CuInS_2$ core. The white LED prepared using these QDs reached an LE of 61 lm/W_{elect} and a CRI of 83. With a similar motivation, Yuan et al. synthesized Cu doped ZnInS/ZnS QDs of which emission color can be tailored by controlling Zn and In concentrations [42]. A white LED was prepared using green-emitting QDs on a blue LED chip. This LED exhibited an LE of 87.2 lm/W_{elect}; however, its CRI remained at 71 and its CCT was 8110 K corresponding to a significantly cool white shade. Later in 2015, the same group synthesized Mn and Cu co-doped ZnInS QDs to realize two-color emission from the dopant states [31]. The green emission in these QDs was associated with the Cu ions while Mn ions were responsible for the reddish emission. The white LED prepared using these QDs reached a CRI of 95 and an LE of 73.2 lm/W_{elect} at a CCT of 5092 K (Fig. 1(g)). Another work addressing this problem was carried out by Zhang et al., who synthesized Cu-doped InP/ZnS/InP/ZnS core/shell/shell/shell QDs [43]. These QDs also exhibited two-color emission; the Cu ions doped into the core of the QDs gave the red emission and the InP shell sandwiched between ZnS layers emitted green color. The white LED constructed by hybridizing these QDs with a blue LED chip acquired a CRI of 91 and a CCT of 5295 K.

At this point, in addition to the literature of semiconductor nanocrystals, the recent developments on phosphor-based nanocrystals, which have sizes smaller than 100 nm and controlled shapes, are worth being highlighted since they share most of the strengths of the Cd-free colloidal nanocrystals. The rare-earth ion-doped phosphor nanocrystals are especially of significance as they allow for excitation in the near-UV regime by increasing the absorption cross sections associated with f–f Judd Ofelt transitions [44] as opposed to their bulk powders excited at shorter wavelengths. With this motivation Dai et al. synthesized ligand-passivated white-emitting Eu-doped Y_2O_3 nanocrystals with quantum efficiencies about ~19% [45]. These phosphors were later integrated with a UV-LED and the LE of the resulting device was 80 lm/W_{elect}. Later Lü et al. reported 2% Dy doped $GdNbO_4$ nanocrystals emitting white light when excited between 350 nm and 390 nm [46]. As an alternative approach, Wang et al. coordinated an organic dye on the surface of Ga_2O_3 nanocrystals and realized white light emission via the energy transfer from these oxide nanoparticles to the dye [47].These white-emitting hybrid nanocrystals exhibited a quantum efficiency of ~30%, a CRI of 95, and a CCT of 5500 K. In another report, boehmite nanoplates having quantum efficiencies up to 58% were employed for high-quality white light generation by Bai et al. [48] These materials were integrated on a UV-LED emitting at 390 nm; the resulting white LED exhibited a CRI of 85.5 and an LE of 6.3 lm/W_{elect}.

One of the important problems of the colloidal solid-state lighting is increasing the light-extraction efficiency from the semiconductor emitters. In a planar architecture, the refractive index of the colloidal semiconductors severely limits the extraction of the light. Therefore, increasing the amount of outcoupled light is very essential to realize high-efficiency light sources. This problem has been addressed for different types of LEDs including organic LEDs [30–32] and epitaxially grown LEDs [52–55] in addition to LEDs using QDs for color conversion [32, 56] and charge injection [57–59]. These works in general make use of scattering structures that alter the exiting angle of the light beam leaving the device and indirectly overcomes the angular limitation imposed on the planar structures by Snell's law. Furthermore, these structures contribute to the angular uniformity of the color-mixing light, especially when small-sized particles are employed [60], which is a desired feature for general lighting applications. In addition, gradually changing refractive index across layered architectures was also employed for improved extraction efficiencies [61]. In principle, there is no obstacle in applying these mature methods to QD-integrated LEDs. In this framework, Diana et al. studied the extraction efficiency of color-converting QD thin films placed on GaN/InGaN quantum wells [56]. It was shown that patterning the GaN/InGaN surface to define a photonic crystal improves the light extraction of the QD film by 40% and also significantly increases the light intensity at off-axis. Alternatively, Dang et al. prepared a nanoporous GaN layer by electrochemical etching [32]. Random texturing of the epitaxial layer was shown to improve the light-extraction efficiency and also constructed an appropriate host for the integration of QDs (Fig. 1(h)). The researchers used these patterns for incorporation of green-emitting and red-emitting QDs on a blue LED. The resulting white LED exhibited a CRI of 74 at a CCT of 6100 K. To improve the light-extraction efficiency of QD-LEDs that are based on electrical charge injection, Yang et al. studied the effect of ZnO nanopillars [57]. In this work, ZnO nanopillars were grown on the LED surface from which the light outcouples. These structures were found to improve the extraction efficiency of the green light produced in the QD-LED by 51.4%. In addition, ZnO nanopillars with a periodicity of 600 nm were observed to increase the off-axis intensities significantly making the light distribution more uniform. Besides these experimental works, recent works estimated the possible improvement on the extraction efficiency using electromagnetic simulations. The results show that it is possible to improve the light-extraction efficiency of the QD-

LEDs by 65% for red-emitting and 34% for blue-emitting devices while making the angular light distribution more Lambertian-like if periodic extraction features made of silica are utilized [59]. In another work, it was shown that employing a high refractive index substrate together with microstructured patterns can enable more uniform angular intensity distribution and improve the extraction efficiency by 80% [58]. These theoretical works show that there is still room for improving the fraction of the outcoupled light from the QD-based LEDs contributing to the overall device efficiency.

3 Electroluminescent devices of colloidal materials for lighting

In this part of the review, we briefly summarize early milestone studies on electroluminescent LEDs of colloids and then continue with reviewing major recent studies. The first electroluminescent devices of semiconductor QDs were developed right after their colloidal synthesis. The early devices borrowed their designs from organic LEDs; however, today original designs involving fully inorganic architectures can be found in the literature. When Colvin et al. reported the first QD-LED in 1994, the electroluminescence was not pure QD emission, instead it resulted simultaneously from CdSe QDs and p-paraphenylenevinylene (PPV) (Figure 2(a)) [62]. The EQE of this LED, which indicates the number of photons obtained from the device per injected charge carrier, remained only at 0.01%; but today pure color LEDs as efficient as 20% [63], which is the limit imposed by Snell's law, are available (see Table 2 for a complete list of EQEs belonging to the QD-LEDs highlighted in this review). However, these efficiencies may be further increased in case improved extraction features are employed.

One of the main problems of the first QD-LED of Colvin et al. was that the charge injecting layers and electroluminescent active region were not isolated enough. This issue was addressed by Coe et al. [69] through sandwiching the QD layer between N,N'-diphenyl-N,N'-bis(3-methylphenyl)-(1,1'-biphenyl)-4,4'-diamine (TPD), which is an organic hole transport layer, and tris-(8-hydroxyquinoline) aluminum (Alq_3), which serves as an electron transport layer. This device reached an EQE of 0.52%, which was the record at its time. Another important step in the QD-LED fabrication was the development of high-quality films of QDs through solvent optimization [70]. This approach was mainly based on the phase separation of two different solvents due to their different vapor pressures causing the formation of large-area hexagonal packing of QDs. Obtaining such high-quality films further improved the EQE of the QD-LED to above 2%.

These early electroluminescent QD-LEDs were single emitters; however, especially for lighting applications there was a need for white QD-LEDs. Anikeeva et al. studied this problem by adjusting the concentration of the QDs of various colors in the monolayer film [71]. The reported device consisted of a hole injection layer (poly(3,4-ethylenedioxythiophene):poly(styrenesulfonate), PEDOT:PSS), a hole transport layer (TPD), QD monolayer film, a hole blocking layer (3,4,5-triphenyl-1,2,4-triazole, TAZ), and an electron transport layer (Alq_3) all coated on the anode in this order. Finally, cathode films of Mg:Ag alloy and Al were coated on these films. The EQE and LE of the white LED became 0.36% and 0.56 lm/W_{elect}, respectively. CRI and CCTs have been measured to be 86 and 5562 K, respectively. Meanwhile, the monochromatic LEDs produced using the same method reached a maximum EQE of 1.6%. Later Anikeeva et al. [64] pointed out that there is a need for a material with reduced highest occupied molecular orbital for achieving higher efficiencies. However, alternative solutions were entailed due to the lack of such candidate materials. The proposed solution was using efficient layers that can nonradiatively transfer their excitons to QDs. Toward this aim, Alq_3, which acts as an exciton sink rather than an exciton source, was replaced by 2,2′,2″-(l,3,5-benzenetriyl)-tris(L-phenyl-l-H-benzimidazole). In addition, the air-sensitive TPD was replaced by spiro-TPD to improve the shelf life of the QD-LED. With this device architecture, EQEs were raised to 0.4%, 0.2%, 2.6%, 2.7%, and 1.0% for blue, cyan, green, orange, and red QD-LEDs (Figure 2(b)). Despite the improved EQEs, the stability of the QD-LEDs at high currents still remained a problem, which was mainly related to organic charge transport layers. Therefore, Caruge et al. replaced the organic charge transport layers with sputtered inorganic metal oxide layers [72] and used NiO and $ZnO:SnO_2$ as the hole and electron transport layers, respectively. These red-emitting QD-LEDs having EQE of 0.1% were capable of working under current densities as high as 3.5 A/cm^2 indicating a significantly improved shelf lifetime.

To identify the reasons for the efficiency reduction at high current densities, an important study was carried out by Shirasaki et al. [2]. In this work, high temperatures during the QD-LED operation, Auger recombination, and quantum-confined Stark effect (QCSE) were investigated as possible candidates causing the efficiency roll-off. The thermal camera measurements at the oper-

Table 1: Colorimetric and photometric performance of the white LEDs using color-converting colloidal materials highlighted in this review.

Color converter	CRI	LER (lm/W_{opt})	LE (lm/W_{elect})	CCT (K)	Reference
Quantum dots	89.2	357	40	2982	Nizamoglu et al. [10]
Phosphor and quantum dots	91.0	-	-	4805	Kim et al. [19]
Quantum dots	92.0	-	-	3442	Liang et al. [20]
Quantum dots	92.0	-	-	5854	Zhang et al. [23]
Quantum dots	90.0	-	46.5	6591	Xuan et al. [24]
Phosphor and quantum dots	81.8	-	58.2	5338	Yoo et al. [28]
Phosphor and quantum dots	81.9	-	91.4	5420	Chen et al. [37]
Quantum dots	95.1	-	95.1	5322	Chen et al. [38]
Quantum dots	94.0	-	34.2	5322	Kim et al. [39]
Quantum dots	95.0	-	54	6500	Yoon et al. [40]
Quantum dots	83.0	-	61	-	Huang et al. [41]
Quantum dots	71.0	-	87.2	8110	Yuan et al. [42]
Quantum dots	95.0	-	73.2	5092	Yuan et al. [31]
Quantum dots	91.0	-	-	5295	Zhang et al. [43]
Phosphor nanocrystals	-	-	80	5418	Dai et al. [45]
Phosphor nanocrystals	95.0	-	-	5500	Wang et al. [47]
Phosphor nanocrystals	85.5	-	6.3	6111	Bai et al. [48]
Quantum dots	74.0	-	-	6100	Dang et al. [32]

CCT, correlated color temperature; CRI, color rendering index; LED, light-emitting diode; LE, luminous efficiency; LER, luminous efficiency of the optical radiation.

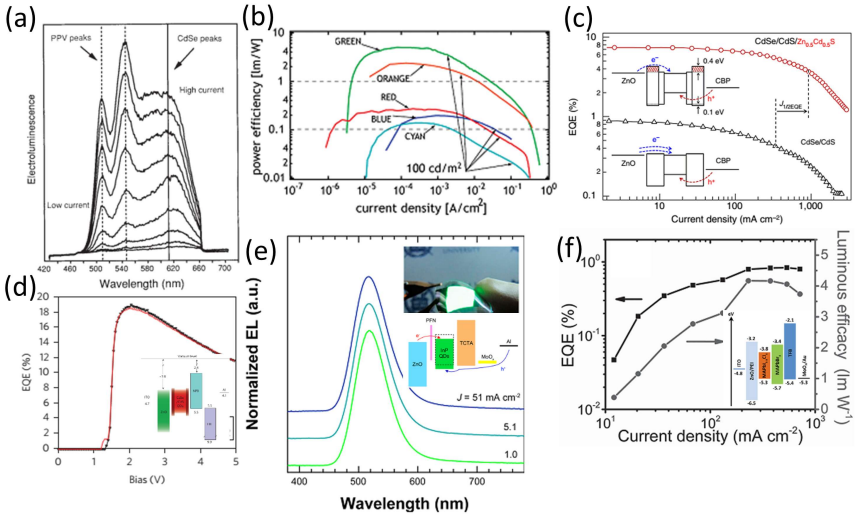

Figure 2: (a) Electroluminescence spectrum of the first electroluminescent quantum dot light emitting diode (QD-LED), in which the QD emission is observed together with the emission of the organic p-paraphenylenevinylene (PPV) layer. Reproduced with permission from Ref. [62], Copyright Nature Publishing Group. (b) Power efficiency (also known as luminous efficiency) of the single color QD-LEDs spanning the whole visible regime. Reproduced with permission from Ref. [64], Copyright American Chemical Society. (c) External quantum efficiency (EQE) of the QD-LEDs made of CdSe/CdS and CdSe/CdS/ZnCdS QDs, which was specifically designed to suppress Auger recombination. Reproduced with permission from Ref. [65], Copyright Nature Publishing Group. (d) EQE as a function of applied bias belonging to the red-emitting QD-LED. Reproduced with permission from Ref. [66], Copyright Nature Publishing Group. (e) Electroluminescence spectra and device structure of a QD-LED made of InP/ZnSeS core/shell QDs. Reproduced with permission from Ref. [67], Copyright American Chemical Society. (f) EQE and luminous efficiency of an electroluminescent nanoplatelets (NPL) LED. Reproduced with permission from Ref. [68], Copyright Wiley International.

ating currents of the QD-LEDs showed temperature increases of only a few degrees, which rules out the high temperature hypothesis. Since the charge retention times of QDs vary from minutes to hours [73], reproducing the EQE measurements after successive measurements within seconds were related to insignificant effect of Auger recombination. On the other hand, a significant correlation was found between the photoluminescence measurements under reverse bias and electroluminescence measurements under the bias of the same magnitude. This showed that the internal electric field across the device has an important effect on decreasing efficiencies at high current densities through QCSE. Another report that came out a few months later, nevertheless, proposes an opposite argument relating this efficiency roll-off to Auger recombination rather than QCSE [65]. This might be related to internal charge accumulation and charging up at the interfaces. Bae et al. observed efficiency decreases at higher current densities in QDs with thicker shells; however, if the QCSEs were dominant, the efficiency roll-off should have occurred at lower current densities in QDs having thicker shells. Furthermore, the time-resolved photoluminescence decays showed distinctly different behavior under positive and negative biases confirming that QCSE is not the dominant effect. They observed that the decay gets faster when positive bias is applied and gets slower under negative bias. Considering the appropriate band alignment with ZnO to transfer their electrons and inappropriate band structure for hole transfer, this behavior is explained by the electron transfer to QDs [74] leading to increased Auger recombination. Based on this analysis, this research team also prepared an electroluminescent QD-LED using CdSe/CdS/ZnCdS core/shell/shell QDs which are specifically designed to partially inhibit electron transfer. This device exhibited significantly improved efficiency roll-off while its EQE increased to 7.5%, which is more than eight times higher than the device fabricated using core/shell QDs (Figure 2(c)). In the same year, the EQE record was pushed to 18% by facilitating a balanced charge injection to the QDs [66]. A good level of charge balance was satisfied by sandwiching the QDs between the ZnO electron transport layer and the spiro-2NPB hole injection layer along with the LG-101 hole injection layer (Fig. 2(d)). The record high EQE of the QD-LEDs was later crowned by Dai et al. in 2014 by adding a thin PMMA layer between the ZnO and the cathode [63]. This extra thin dielectric layer weakened the electron transfer and helped the device to improve the balance of the injected charges, in addition to avoiding possible plasmonic quenching of QDs in the proximity of the ZnO layer. As a result, the efficiency roll-off was significantly eliminated and the EQE reached 20%, which is the theoretical maximum for planar devices without extraction features. To address the efficiency roll-off issue, Dong et al. recently proposed the use of a Cs_2CO_3 layer for hole-blocking together with an electron injecting a ZnO nanoparticle layer [75]. This red-emitting device surpassed the brightness of organic LEDs at a value of 165,000 cd/m^2 at 1000 mA/cm^2 current density.

Due to the eco-unfriendly nature of Cd-based QDs, electroluminescent devices of Cd-free QDs were heavily investigated. The first demonstration of the Cd-free QD-LED dates back to 2011, in which Lim et al. used InP/ZnSeS core/gradient-shell QDs with quantum efficiencies >50% [76]. Despite relatively high quantum efficiencies of these QDs, they lacked tunability of the emission spectrum and exhibited a very broad emission with full width at half-maximum values reaching 70 nm. The LED made from these QDs had an EQE of only 0.008%. Later in 2012 Yang et al. synthesized InP/ZnS QDs with quantum efficiencies >60% and their emission color could be controlled over the whole visible regime [77]. A white LED with a CRI of 91 was fabricated using these QDs; the blue-green emission of this device originated from the poly-TPD hole transport layer while the red emission at 600 nm stemmed from the InP/ZnS QDs. Later in 2013 Lim et al. synthesized InP/ZnSeS core/gradient-shell QDs having quantum efficiencies >70% [67]. The fabricated QD-LEDs exhibited an EQE of 3.46%, which is 10 times better compared with the previous best device, and delivered a maximum brightness of 3900 cd/m^2, which was five times better compared with the previous state-of-the-art device (Fig. 2(e)).

In addition to QDs, solution-processed perovskites have very recently been used in LEDs because they enable narrow-band emission and have high quantum efficiencies. One of the first electroluminescent LEDs made of perovskites was reported by Tan et al. in 2014 [78]. In this work, infrared and green LEDs were prepared using solution-processed $CH_3NH_3PbI_{3-x}Cl_x$. Electroluminescent devices of these materials were prepared by sandwiching them between large band gap titanium dioxide and poly(9,9′-dioctylfluorene) (F8) layers. Here, titanium dioxide serves as an electron injection as well as a hole-blocking layer while F8 was used to confine the holes within the perovskite layer and block the electron flow. The infrared perovskite LED reached an EQE of 0.76% and a radiance of 13.2 Wm^{-2}sr^{-1} while the green-emitting perovskite LED had an EQE of 0.1% with an illuminance of 364 cd/m^2. In the same year, Kim et al. reported an LED spanning the whole visible regime by compositional control of solution-processed $CH_3NH_3PbCl_xBr_yI_{3-x-y}$ perovskites [79]. In

this work, a buffer hole injection layer composed of PEDOT:PSS and tetrafluoroethylene-perfluoro-3,6-dioxa-4-methyl-7-octene-sulfonic acid copolymer (PFI) was utilized to obtain a gradually increasing work function thanks to the self-organization of PFI. This work function modification helped to decrease the hole injection barrier between PEDOT:PSS and the perovskite, allowing for better hole injection and electron blocking. An additional benefit of this PFI incorporation has been the prevention of exciton quenching at the interface of hole injection and perovskite layers. These green-emitting devices reached an EQE of 0.125% and a luminance level of 417 cd/m^2 with an extraordinary narrow band-emission of 20 nm. In 2015, Jaramillo-Quintero employed solution-processed $CH_3NH_3PbI_{3x}Cl_x$ to obtain a deep-red perovskite LED [80]. In the device configuration, TiO_2 and Spiro-OMeTAD (2,2′,7,7′-tetrakis(N,N-di-p-methoxyphenylamine)-9,9-spirobifluorene) served as electron and hole injection layers, respectively, while no electron and hole transport layers were utilized. This LED exhibited a radiance of 7.1 Wsr^{-1}m^{-2} and a maximum EQE of 0.48%. Later Li et al. proposed the formation of the perovskite layer by blending the nanocrystalline perovskites with a dielectric polymer to obtain a smooth perovskite layer without electrical shunts and simultaneously to realize a charge-blocking structure [81]. The electroluminescent LED was constructed by sandwiching this perovskite layer between F8 serving as an electron transport and a hole-blocking layer and PEDOT:PSS serving as a hole-injection layer. This green-emitting device reached an EQE of 1.2%, which is two orders of magnitude larger than the device without dielectric polymer. In the work of Wang et al., this film-formation problem was addressed by incorporating a ZnO film within polyethylenimine [68]. This enabled the formation of high-quality perovskite ($CH_3NH_3PbI_{3-x}Cl_x$) thin films and serves as a low work-function cathode for electron injection (Fig. 2(f)). The deep-red-emitting device exhibited an EQE of 3.5% at 160 mA/cm^2 current density with a maximum radiance reaching 28 Wsr^{-1}m^{-2}.

Recently, colloidal quantum wells of semiconductor nanocrystals also known as NPLs were employed as active layers of LEDs. In the work of Chen et al. [82] CdSe/$Cd_{0.7}Zn_{0.3}S$ NPLs were used as the emissive layer, which was placed on top of the hole-injecting PEDOT:PSS and hole-transporting PVK layers. Subsequently, ZnO was utilized on top of the NPLs as the electron transport layer. The resulting red-emitting device exhibited an EQE of 0.63% with a maximum luminance of 4499 cd/m^2. Furthermore, the electroluminescence spectrum of these NPLs showed a full width at half-maximum of only 27 nm. In the same year Vitukhnovsky et al. demonstrated an LED using CdSe NPLs [83]. In this work, the NPLs were placed on top of PEDOT:PSS and TPD hole injection and transport layers, respectively. TAZ (3-(Biphenyl-4-yl)-5-(4-tert-butylphenyl)-4-phenyl-4H-1,2,4-triazole) was coated on the NPLs as the electron transport layer. This device had a turn-on voltage at 5.5 V and the emission peak was located at 515 nm with a bandwidth of only 10 nm. A red-shift of 8 nm was observed compared with the photoluminescence peak, which was attributed to the QCSE. Later, Fan et al. reported an electroluminescent LED with emission bandwidths as narrow as 12.5 nm [84]. In this work, the emission spectra of the NPLs were controlled by tuning the Se/S ratio within alloyed NPLs in the range of 481–513 nm. To fabricate an electroluminescent device, these NPLs were coated on top of the ZnO electron transport layer. Following the spin-coating of the NPLs, 4,4′-bis(N-carbazolyl)-1,1′-biphenyl and MoO_3 were coated as the hole transport and injection layers, respectively. The bandwidths of the emission spectrum were found to decrease with increasing emission wavelengths; and the narrowest emission of 12.5 nm was obtained when the emission peak was at 520 nm. Nevertheless, the EQE of this device was not reported.

Table 2: Summary of the external quantum efficiency (EQE) belonging to the electroluminescent light-emitting diodes (LEDs) covered in this review.

Active material	EQE (%)	Reference
Quantum dots	0.01	Colvin et al. [62]
Quantum dots	0.52	Coe et al. [69]
Quantum dots	>2	Coe-Sullivan et al. [70]
Quantum dots	0.36	Anikeeva et al. [71]
Quantum dots	0.2–2.7	Anikeeva et al. [64]
Quantum dots	0.1	Caruge et al. [72]
Quantum dots	7.5	Galland et al. [74]
Quantum dots	18	Mashford et al. [66]
Quantum dots	20	Dai et al. [63]
Quantum dots	0.008	Lim et al. [76]
Quantum dots	3.46	Lim et al. [67]
Perovskites	0.1	Tan et al. [78]
Perovskites	0.125	Kim et al. [79]
Perovskites	0.48	Jaramillo-Quintero et al. [80]
Perovskites	1.9	Li et al. [81]
Perovskites	3.5	Wang et al. [68]
Nanoplatelets	0.63	Chen et al. [82]

4 Colloidal materials for color enrichment in displays

The colloidal materials have inherently important advantages for display applications. One of their most important strengths is the narrow band emission, which broadens the color gamut of the displays significantly. Another attractive feature of the colloidal materials is the precise control of the emitted color so that the desired colors can be addressed by the size and shape control of the emitters. Finally, the high quantum efficiencies obtained in recent years have brought these materials into the focus of display applications.

One of the first works employing colloidal materials in displays was reported in 2010 by Jang et al. from Samsung. In this work, the research team employed green-emitting CdSe/ZnS/CdSZnS and red-emitting CdSe/CdS/ZnS/CdSZnS colloidal QD nanocrystals in liquid crystal displays for color enrichment [85]. The synthesized QDs used in this study exhibited near-unity quantum efficiencies in solution. When they were integrated on an LED after hardening within silicone, this quantum efficiency was observed to drop to 72% and 34% for green-emitting and red-emitting QDs, respectively. The researchers blended these QDs and encapsulated them within silicone on a blue LED. The resulting white LED, which was used as the backlight of a 46 inches display, reached an LE of 41 lm/W_{elect} at a CCT of 100,000 K. The obtained color gamut fully reproduced the standards of the National Television Standards Committee (NTSC) and easily surpassed the color gamut that can be defined by phosphor-integrated LEDs. The spectrum of this white LED and its color gamut are presented in Fig. 3(a), and a photograph of the display is given in Fig. 3(b).

Later in 2012, Chen et al. successfully decreased the strong luminescence of the excitation source by recycling the excitation photons using distributed Bragg reflectors (DBRs) made of HfO_2/SiO_2 [86]. In this work, the researchers used an UV LED to pump the spray-coated pixelated red/green/blue QDs and also white-emitting blended QD film for color enrichment (Fig. 3(c)). Subsequently, the DBR was coated on top of the color enrichment film (Fig. 3(d)). This DBR layer was designed to have a stop band at 400 nm with a bandwidth of 60 nm so that the light coming from the UV LED can be recycled to excite the QDs more strongly. As a result, more than four times the intensity enhancement was realized for red emission while the enhancements for green and blue were more than twice and more than thrice, respectively, compared with the color enrichment without DBR layers (Fig. 3(e)). Thanks to the narrow bandwidth of the QDs, the color gamut of the pixelated color enrichment reached 120% of the NTSC color gamut.

In addition to the experimental studies employing QDs for color enrichment in LCDs, it is also important to identify the spectral features of QDs that can offer improved color definition. To address this need, Luo et al. [87] carried out a theoretical study and determined the necessary amplitude, peak emission wavelength, and full width at half-maximum of QD emission to realize high brightness of the light transmitted through LCD color filters along with a larger color gamut both in CIE 1931 and 1976 color spaces. In this work, the authors simulated the performance of the display by varying the peak emission wavelengths and bandwidths of the blue LED along with green-emitting and red-emitting QDs. The minimum bandwidth for the LED chip was assumed to be 20 nm while that of the QDs was assumed to be 30 nm. The results showed that there is a trade-off between the color gamut and the brightness after considering the transmission spectra of the color filters. As expected, the emitters with narrow emission bandwidths increase the obtained color gamut; however, at the same time this decreases the total overlap with the human eye sensitivity function for the red and blue emitters because of the accompanying shift of the peak emission wavelengths away from 550 nm where the human eye is most sensitive. Therefore, increasing the color gamut comes at the cost of reduced brightness. Considering all these factors, Luo et al. showed that it is possible to improve the color gamut of the LCD with QD color enrichment by 20% compared with NTSC if the respective peak emission wavelengths of the blue, green, and red components are 447.6 nm, 523.5 nm, and 634.8 nm. Corresponding bandwidths are 20 nm, 30 nm, and 30 nm, while the relative amplitudes are 37.3%, 27.8%, and 34.9%, respectively.

In recent years, while the semiconducting colloidal perovskites have attracted significant attention for light-harvesting applications, their high photoluminescence quantum yields allowed for their use in light-emitting devices. For example, in 2015 Zhang et al. synthesized $CH_3NH_3PbX_3$ (X = Br, I, Cl) perovskite nanocrystals having quantum efficiencies reaching 70% [88]. In addition to this, the synthesized materials allowed for obtaining a very saturated green color because of their emission bandwidths of 21 nm, which are significantly smaller than the available Cd-based QDs and much narrower than those of In-based Cd-free QDs. This narrow emission together with the high quantum efficiency makes these perovskites suitable materials for color enrichment in LCDs. To benefit from these feature of perovskites, the authors hybridized green-emitting perovskites with red-emitting $K_2SiF_6:Mn^{4+}$

phosphor on a blue LED chip (Fig. 3(f)). Thanks to their narrow emission, the proposed device covered an area of 130% of the NTSC color gamut indicating a significant improvement in the color definition of the displays.

To push the efficiencies further while realizing even narrower emitters, Protesescu et al. synthesized Cs-based perovskites [89]. These monodisperse nanocrystals of perovskites varying in size from 4 nm to 15 nm reached quantum efficiencies up to 90%. At the same time, their full width at half-maximum values became as narrow as 15 nm. Furthermore, these nanocrystals successfully spanned the whole visible wavelengths through controlling the material composition. The researchers incorporated these materials into PMMA films and suggested their use for display color enrichment (Fig. 3(g), inset). Thanks to their narrow emission bandwidths, these perovskite nanocrystals offer a color gamut of 40% beyond the NTSC standard (Fig. 3(g)).

5 Electroluminescent displays of colloidal materials

The electroluminescence of colloidal semiconductors has also attracted significant attention for display applications. This is basically because of their color tunable, narrow-band emission spectra along with high quantum efficiencies. Different from the color enrichment applications of colloidal materials, their electroluminescent devices may remove the need for color filters and polarizers if pixelated LEDs are utilized. Therefore, they may offer overall high efficiencies if stability issues are addressed and extraction efficiencies are increased.

One of the first applications of the electroluminescent QD-displays dates back to 2008. In the work of Kim et al. the green-emitting and red-emitting QDs were integrated into an electroluminescent device structure [90]. The blue emission was obtained from TPD that also acts as the hole transport layer for QDs. The pixelated structure was obtained by contact printing and the critical distance between the pixels has been 25 μm corresponding to a resolution of 1000 pixels-per-inch (ppi). The electroluminescent device was produced first by spin-coating PEDOT:PSS as the hole injection layer. Later, TPD was coated as the hole transport layer and also the blue-emitting layer in the pixels where no QD was employed. Subsequently, QDs were integrated to the device structure by contact printing. TAZ was used for blocking the holes and Alq_3 was employed as the electron injection layer. Finally, the Ag:Mg and Ag layers were used as the cathode of the device. This device reached an EQE of 1.2% for the red component while those of the green and blue components were 0.5% and 0.2% respectively (see Table 3 for a list of EQEs and brightnesses of the electroluminescent displays reviewed here). Another research team from Samsung Electronics also worked on the development of contact printed QD displays [91]. This team produced rectangular patterns of red, green, and blue QDs sandwiched into an LED device structure. The display size of the device was 4 inches with a resolution of 100 ppi and the brightness was as high as 16,380 cd/m^2. The efficiencies of the printed QD-LEDs were improved by 25–52% compared with the control devices fabricated using spin-coating. In this work, the efficiency of the green LED was further improved using plasmonic interaction. For this purpose, silver nanoparticles were printed at a distance of 11–12 nm from the QD layer and 71% enhancement in the power efficiency of the green-emitting device was realized. An image shown on the fabricated display is given in Fig. 4(a). In 2015, Choi et al. further developed this methodology using the intaglio printing technique to produce high-resolution QD displays [92]. In this work, the electroluminescence of blue, green, and red QDs was realized within a wearable device having a resolution up to 2460 ppi corresponding to a pixel size of 6 μm (Fig. 4(b)). This device reached a brightness of 14,000 cd/m^2 at 7 V and had an EQE of 1.5%. Furthermore, the performance of this device was still maintained after 1000 deformation tests.

Ink-jet printing is another attractive technique for QD-LED fabrication because of its simplicity, cost-effectiveness, and high production speed. This technique was employed by Haverinen et al. in QD displays [93] to define a 640 × 480 pixels geometry using standard photolithography techniques. Each pixel acquired an area of 19,600 μm^2 with a pixel separation of 80 μm. The blue, green, and red-emitting QDs were ink-jet printed into these areas. The EQEs of these devices turned out to be 0.23%, 0.15%, and 0.1%, respectively for red, green, and blue QD LEDs. Recently, QD LEDs have been fabricated using 3D printing technique by Kong et al. [94] In this device, the LED was built up on an UV-adhesive substrate by facilitating organic polymers as charge transport layers (PEDOT:PSS and Poly-TPD), solid and liquid metals for contacts, and QDs as the active layer. The maximum brightnesses of green-emitting and orange-emitting devices were measured to be 250 cd/m^2 and 70 cd/m^2, respectively.

In 2015 Kim et al. employed electrohydrodynamic jet printing to obtain high resolution patterns of electroluminescent QDs [95]. The researchers successfully tailored the thickness of the QD layers by controlling the nozzle

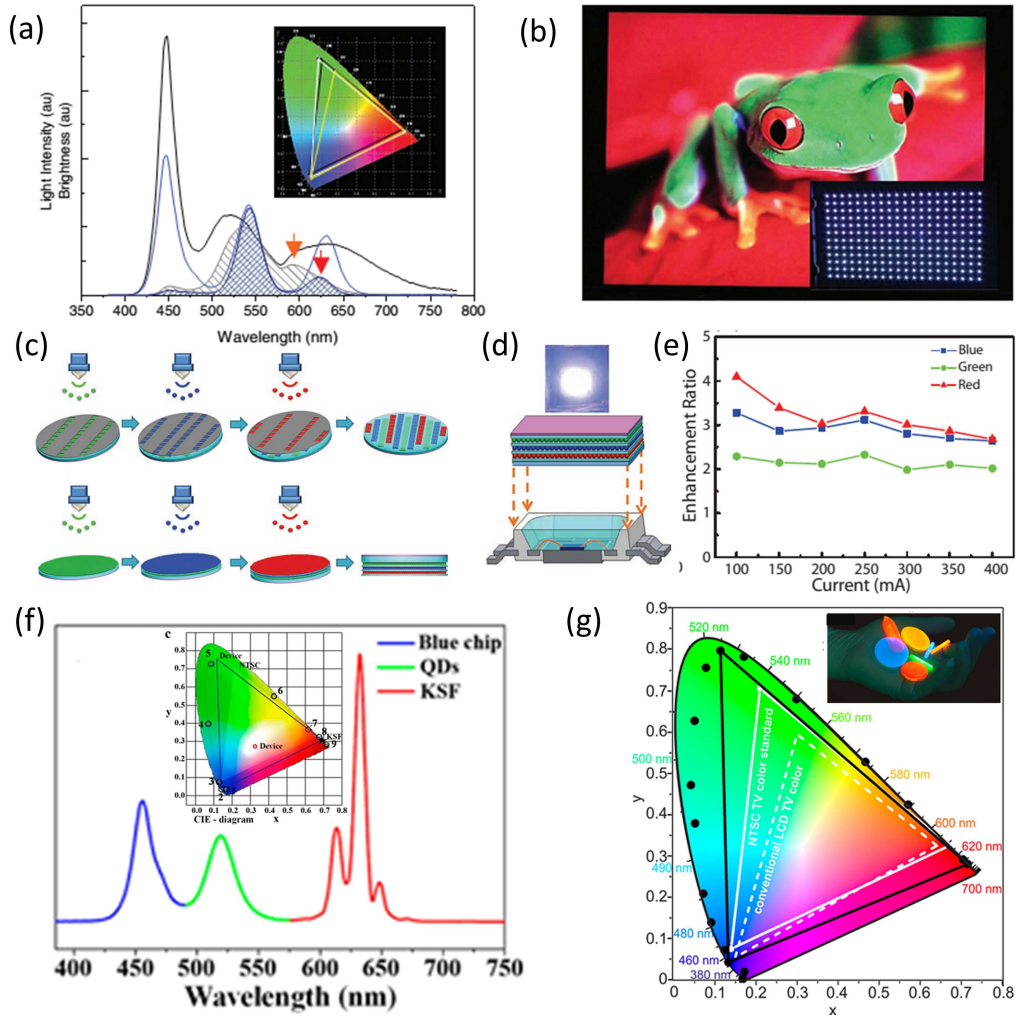

Figure 3: (a) Spectrum of the white light-emitting diode (LED) fabricated using quantum dot (QD) films on a blue LED chip along with the National Television Standards Committee (NTSC) color gamut (inset, yellow triangle) and the color gamut of the produced white LED (inset, white triangle). (b) Display image of 46 inches display. Reproduced with permission from Ref. [85], Copyright Wiley International. (c) Fabrication methodology of the QD color enrichment produced using spray coating. The upper image shows the production of pixelated films while the lower image illustrates the fabrication of all-color white color enrichment film. (d) A schematic of a white LED whose emission was improved using distributed Bragg reflector (DBR) layers on top of the color enrichment film. (e) Enhancement factors for each color component. Reproduced with permission from Ref. [86], Copyright Wiley International. (f) Emission spectrum of the display backlight produced by hybridizing a blue LED chip with the green-emitting perovskite and red-emitting phosphor. The color gamut is presented with the black triangle in the inset. Reproduced with permission from Ref. [88], Copyright American Chemical Society. (g) Chromaticity points of the Cs-based perovskites of colors spanning the whole visible regime. The black triangle represents the color gamut of the suggested perovskite display. The inset shows the films of these perovskites in poly(methyl methacrylate) (PMMA) under ultraviolet illumination. Reproduced with permission from Ref. [89], Copyright American Chemical Society.

size, stage speed, ink composition, and bias voltage. Thicknesses down to 25 nm with pixel widths of 250 nm could be reproducibly realized. To obtain an electroluminescent device, the research team used PEDOT:PSS as the hole injection layer and poly[(9,9-dioctylfluorenyl-2,7-diyl)-co-(4,40-(N-(4-s-butylphenyl)) diphenylamine)] as the hole injection layer. Subsequently, the QDs were placed on these layers via electrohydrodynamic jet printing and the ZnO layer, serving as the electron transport layer, was coated. Finally, Al was evaporated to serve as the cathode. The maximum EQE of the green QD-LED was 2.5% while that of the red LED was 2.6%. The electroluminescence of the QD LED and its device architecture are presented in Fig. 4(c) and 4(d), respectively.

In addition to the pixelated QD-displays, electroluminescent QD-LEDs were also employed as backlight in LCDs. One of these devices was demonstrated by Bae et al., where red, green, and blue QDs were mixed and then spin-

coated [96]. Subsequently, researchers employed this device as the backlight of a 1.2 inch × 1.2 inch LCD (Fig. 4(e)). This QD-LED reached a brightness of 6400 cd/m^2 at the current density of 250 mA/cm^2. The LE of this device has been between 1.5 lm/W$_{elect}$ and 2.4 lm/W$_{elect}$ with EQEs between 1.0% and 1.3%. Similar to this work, Oh et al. [97] fabricated a blue-emitting QD-LED, but in this work green-emitting and red-emitting phosphors were placed on the front face of the LED and white light emission was realized with the photoluminescence of the phosphors excited by the electroluminescent blue QDs. This device structure exhibited brightnesses of 1570 cd/m^2, 12920 cd/m^2, and 3120 cd/m^2 for blue, green, and red color components, respectively, with respective EQEs of 6.8%, 2.8%, and 2.0%. Due to the emission bandwidth of the phosphors used in this work, the color gamut of the suggested display remained at 82% of the NTSC standard.

Table 3: External quantum efficiency (EQE) and brightness values of the quantum dot based electroluminescent displays covered in this review.

Reference	EQE (%)	Brightness (cd/m^2)
Kim et al. [90]	0.2–1.2	>100
Kim et al. [91]	-	423–16,380
Choi et al. [92]	1.5	14,000
Haverinen et al. [93]	0.1–0.23	122–352
Kong et al. [94]	-	70–250
Kim et al. [95]	2.5–2.6	11,250–36,000
Bae et al. [96]	1.0–1.3	6390
Oh et al. [97]	2.0–6.8	1570–12,920

6 Lasers of colloidal materials

The developments on high-quality semiconductor colloidal nanoparticle synthesis have also paved the way for their application in lasers. Especially their low cost and color tunability offer significant advantages over the epitaxially grown gain media. However, difficulties in making highly packed dense films out of these materials significantly complicates the gain process; but these complications still do not make the lasing impossible.

The optical mechanisms of QD lasing were studied in detail by Klimov et al. [17] In this work, they emphasized that the main obstacle for lasing is the competition between nonradiative and radiative losses. The optical gain within a spherical QD requires the average number of electron-hole pairs (N) to be at least unity. If the electronic structure and biexcitonic states are taken into account, this number increases to 1.5 [98]. Today, the synthesis of high-quality QDs mostly eliminated the radiative recombination problem but the Auger recombination still requires special QD composition engineering. Considering the fact that Auger recombination is more dominant in smaller sizes [99], the electron-hole pair lifetime is mainly dictated by the Auger mechanism at high excitation power. Therefore, population inversion can be obtained only if the relaxation to the ground state occurs faster than the Auger recombination [17]. This can be accomplished if the QDs having larger gain cross sections are utilized and if they are assembled in very dense films. Furthermore, the use of ultrafast optical pumping can be helpful for population inversion as well [100].

One of the first demonstrations of QD lasing was reported by Eisler et al. in 2002 [100] In this work, CdSe QDs were stabilized inside sol-gel titania waveguides. The spin coated film of this mixture was pumped with a laser having a pulse width of 100 fs peaking at 400 nm. A clear amplified spontaneous emission was observed from this film, which was signified with the decreasing full width at half-maximum of the QD emission from 28 nm to 7 nm. Subsequently, distributed feedback gratings were prepared by reactive ion etching of silica layer on silicon substrate and the titania-QD film was spun on this grating. The resulting structure allowed for the lasing of the red QDs (Fig. 5(a)). In the same year, Marko et al. demonstrated the lasing of the QDs inside microcapillary tubes [101]. These microcavities can support planar waveguide modes developing along the tube length and also whispering gallery modes around the inner circumference of the tube. Since there is no feedback along the tube, only amplified spontaneous emission could be observed; but the feedback action provided by the whispering gallery modes allowed for micro ring lasing at an excitation fluence of 1.25 mJ/cm^2 (see Table 4 for a list of lasing thresholds of colloidal lasers discussed in this review). Later, Chan et al. demonstrated blue QD lasing by employing CdS/ZnS QDs [102]. These QDs were spin-coated by embedding into silica sol-gel matrix in the presence of silica spheres to obtain a spherical resonator. By pumping these QDs with a 100 fs laser at 400 nm, blue QD lasing was observed at an excitation fluence of 3.7 mJ/cm^2. In 2009, Zhang et al. employed two-photon absorption to achieve QD lasing [103]. In this work, spherical resonators of porous silica microspheres were used as the feedback mechanism. The QDs were doped into the pores of these micro beads and excited by a titanium:sapphire laser emitting at 800 nm. These QD-doped silica micro beads were

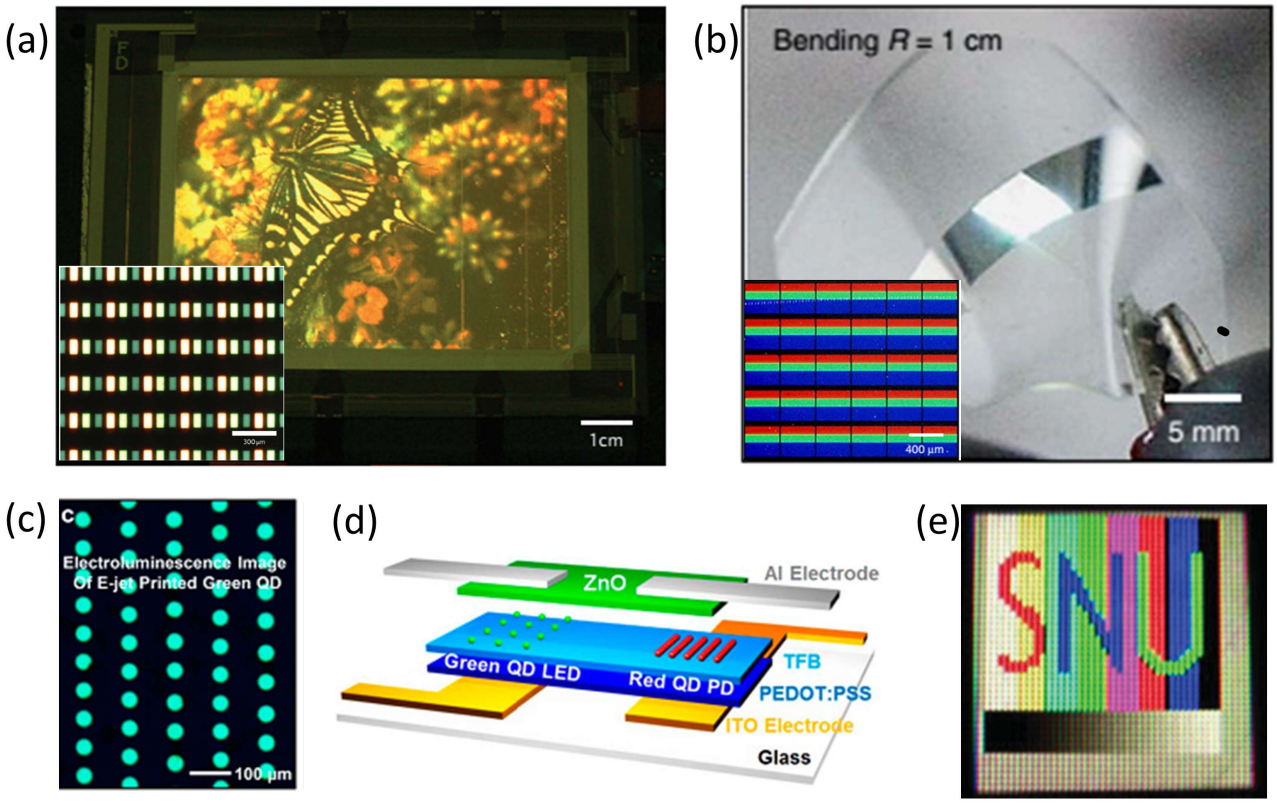

Figure 4: (a) A butterfly image illustrated by the electroluminescence of quantum dot (QD) display. Inset shows a close look at the electroluminescent display. Scale bars are 1 cm for the larger photograph and 300 μm for the inset image. Reproduced with permission from Ref. [91], Copyright Nature Publishing Group. (b) Real color photograph of wearable QD display and the electroluminescence of the pixels (inset). Reproduced with permission from Ref. [92], Copyright Nature Publishing Group. (c) Electroluminescence of the green QD light-emitting diode (LED) produced by electrohydrodynamic jet printing and (d) illustration of the device structure. Reproduced with permission from Ref. [95], Copyright American Chemical Society. (e) Trichromatic QD LED backlit LCD unit. Reproduced with permission from Ref. [96], Copyright Wiley International.

shown to exhibit lasing at ~610 nm starting from an excitation fluence of 0.5 mJ/cm^2.

In 2012, Dang et al. used specifically engineered QDs to realize blue-emitting, green-emitting, and red-emitting vertical cavity surface-emitting lasers [98] (Fig. 5(b) and (c)). In this work, CdSe/ZnCdS core/shell QDs were employed to enable Stokes shift between the absorption and the emission spectra that further helps to minimize the effect of the Auger recombination. The high quantum efficiencies reaching 80% within high-density QD films also helped in the realization of laser operation. DBRs that sandwich the spin-coated QD films were utilized as the feedback mechanism in the laser. The suppressed Auger recombination helped to decrease the amplified spontaneous emission thresholds to 90 μJ/cm^2, 145 μJ/cm^2, and 800 μJ/cm^2, for red, green, and blue, respectively, and the lasing threshold for the red QDs have been reported as 60 μJ/cm^2.These values for green and red were an order of magnitude smaller than that of the previous reports. Later, this group employed these QDs on distributed feedback gratings to achieve lasing [104, 105] with power conversion efficiencies reaching 28% for the red lasers [105]. An interesting study on the lasing of QD solution was reported by Wang et al. [106] In this work, blue-emitting CdZnS/ZnS ternary alloyed QDs were synthesized to obtain high-efficiency emitters with suppressed Auger recombination. These QDs were later incorporated into hollow fused silica fibers, in which whispering gallery modes provided the feedback mechanism required for lasing. The quasi-continuous pumping of the QDs by a laser having a pulse width of 5 ns showed lasing after an excitation energy of 25.2 mJ/cm^2.

After the work of Zhang et al. [93], the use of the QDs as gain media based on two-photon and three- photon absorption continued to be an important topic of attraction. For example, Guzelturk et al. [110] synthesized

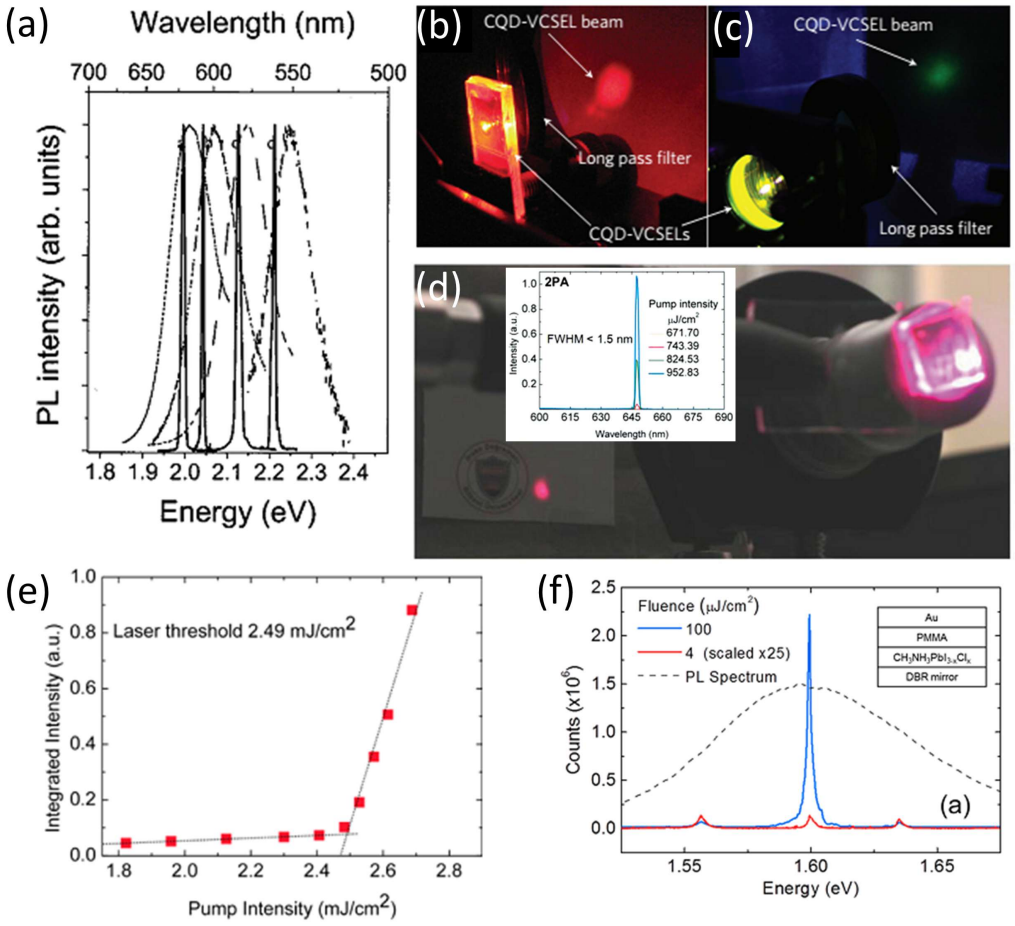

Figure 5: (a) Photoluminescence spectra of the quantum dots (QDs) between distributed Bragg reflector (DBR) layers below (dashed lines) and above lasing threshold. Reproduced with permission from Ref. [100], Copyright American Institute of Physics. Real color photographs of (b) red-emitting and (c) green-emitting QD lasers. Reproduced with permission from Ref. [98], Copyright Nature Publishing Group. (d) Real color photograph of all-colloidal QD-laser and its emission spectrum (inset). Reproduced with permission from Ref. [107], Copyright Wiley International. (e) Integrated photoluminescence of the nanoplatelet (NPL) laser as a function of the excitation fluence. Reproduced with permission from Ref. [108], Copyright American Chemical Society. (f) Photoluminescence spectrum of the perovskite laser below (dashed line) and above (continuous lines) lasing threshold. Reproduced with permission from Ref. [109], Copyright American Chemical Society.

CdZnS/CdS core/gradient shell QDs so that Auger recombination could be weakened. In this work, a record low two-photon absorption-pumped amplified spontaneous emission threshold of 6 mJ/cm^{2}was achieved for the blue QDs, and this value was 60 μJ/cm^2 for one photon-absorption regime. Similarly, Wang et al. synthesized orange-emitting CdSe/CdS/ZnS QDs having a quasi-type-II band alignment [111]. This energy band engineering allowed for improving the three-photon absorption cross section as well as suppression of Auger recombination and three-photon-induced random lasing was successfully demonstrated for the first time. In 2015, vertical-cavity surface emitting lasers employing only colloidal nanoparticles were demonstrated by Guzelturk et al. [107] In this cited work, multiple layers of titania and silica nanoparticles were spun to obtain a DBR that will provide the feedback for laser action. The gain medium in this work consisted of relatively small-sized CdSe/CdS core/shell QDs, which exhibit high photoluminescence quantum efficiencies. The amplified spontaneous emission thresholds of these red-emitting QDs were measured to be 29 μJ/cm^2 and 5.02 mJ/cm^2 for one-photon and two-photon absorption regimes, respectively. Subsequently, these materials were sandwiched between the DBR layers and stable lasing operation was successfully demonstrated after a two-photon pumped excitation fluence of 764 μJ/cm^2 (Fig. 5(d)).

Thanks to their high two-photon-absorption cross sections, nanorods were employed in lasers as well. For example Xing et al. reported a nanorod laser by using CdSe/CdS core-seeded nanorods [112]. These red-emitting

nanorods were coupled to a microspherical cavity and single mode lasing was reported at excitation energies as low as 0.99 mJ/cm^2. Gao et al. reported a nanorod laser which also exhibits polarization anisotropy [113]. In this work, CdSe/CdS nanorods were coated on the inner wall of a capillary tube. Despite the existence of whispering gallery mode, polarized gain was found to stem from the alignment of the nanorods, not from the whispering gallery modes. The lasing threshold energy was 5.2 μJ for both the TE and TM polarizations; however, with the increasing excitation energy the degree of polarization becomes 0.72 which corresponds to a polarization ratio of 6.1. In another work, Di Stasio et al. [114] used the coffee-stain effect to realize lasing action with water soluble CdSe/CdS nanorods having a large CdS diameter, which decreased the effects of surface defects during the ligand exchange. The films of these nanorods had an amplified spontaneous emission threshold of 130 μJ/cm^2. To benefit from the coffee-stain effect as the feedback mechanism, these nanorods were drop-casted and this laser exhibited a threshold of 10 μJ/cm^2.

Owing to their large optical cross sections, slow Auger recombination rates, and narrow emission bandwidths, NPLs are also important candidates for obtaining efficient gain media. The first demonstrations of stimulated emission with colloidal NPLs were reported independently by She et al. [115] and Guzelturk et al. [108]. In the work of She et al., CdSe NPL films were spun on glass substrate; the threshold for amplified spontaneous emission was measured to be 17 μJ/cm^2, which was lower than the lowest threshold obtained using QD films [98, 116]. Thresholds down to 6 μJ/cm^2 were obtained when CdSe/CdS core/shell NPL heterostructures were employed. Simultaneously, Guzelturk et al. demonstrated lasing action from CdSe and CdSe/CdS core and core/crown NPLs and systematically studied their optical gain performance. The authors observed that core/crown NPLs achieve improved gain performance compared with only core NPLs because of the increased absorption cross section and efficient interexciton funneling from CdS crown to CdSe core. This achieved a record low single-photon pumped amplified spontaneous emission threshold of 41 μJ/cm^2 at the time. A vertical-cavity surface emitting laser was fabricated using core/crown NPLs sandwiched between DBRs made of silica and titania nanoparticles (Fig. 5(e)). Also, two-photon pumped lasing accomplished for the first time and the corresponding lasing threshold was measured to be 2.49 mJ/cm^2. Later, Olutas et al. studied the dependence of the amplified spontaneous emission thresholds on lateral size in one-photon and two-photon absorption regimes [117]. The results showed that larger NPL sizes exhibit larger thresholds in the one-photon absorption regime due to increasing defect population. However, the threshold in the two-photon absorption regime turned out to be decreasing in larger NPLs, which was attributed to the significantly large two-photon absorption cross section measured for the first time to be >10^6 GM. The demonstration of the first continuous-wave excited lasing was subsequently reported by Grim et al. in 2014 [118] In this work, the CdSe NPL thin films were shown to have a stimulated emission threshold of 6 μJ/cm^2 under femtosecond pulse excitation and continuous-wave lasing was observed using these NPL films sandwiched between DBRs reportedly at 440 W/cm^2 excitation power.

In addition to QDs, nanorods, and NPLs, perovskites, which are considered as the rising star of the emerging photovoltaics, were also employed in lasing applications. Although these perovskites used for lasing are not nanocrystalline colloids, we include them in our review because of their high performance. In 2014, Xing et al. demonstrated amplified spontaneous emission using solution processed $CH_3NH_3PbX_3$ (X=Cl, Br, I) perovskites [119]. Thanks to their large absorption coefficients, very low bulk defect densities, and slow Auger recombination rates, the threshold of the amplified spontaneous emission was measured to be 12 μJ/cm^2. Later, Deschler et al. employed solution-processed $CH_3NH_3PbI_{3-x}Cl_x$ perovskites having a quantum efficiency of 70% within a vertical-cavity surface emitting laser [109] (Fig. 5(f)). The cavity was constructed using a commercially available dielectric mirror and a gold top mirror. The lasing threshold was measured to be 0.2 μJ/pulse; furthermore, different from the QDs and nanorods, no shift in the stimulated emission was observed. This may suggest that the lasing occurs not due to a biexciton action, instead a single exciton action is dominant. Finally, Sutherland et al. grew perovskites using the atomic layer deposition technique on glass for amplified spontaneous emission measurements and on silica microspheres for lasing [120]. For the growth of perovskite, a thin film of PbS was used as the seed layer; subsequently, $CH_3NH_3PbI_3$ perovskites were grown through the reaction of the PbS layer with I_2 gas and later with CH_3NH_3I. The amplified spontaneous emission threshold of this film on glass was measured to be 65 μJ/cm^2, while the lasing threshold of the films grown on silica microspheres turned out to be 75 μJ/cm^2.

Table 4: Lasing thresholds of the colloidal lasers highlighted in this review.

Gain medium material	Lasing threshold ($\mu J/cm^2$)	Reference
Quantum dots	1250	Malko et al. [101]
Quantum dots	3700	Chan et al. [102]
Quantum dots	500	Zhang et al. [103]
Quantum dots	60	96
Quantum dots	25200 (Quasi-continuous pumping)	Wang et al. [106]
Quantum dots	764	Guzelturk et al. [107]
Nanorods	990	Xing et al. [112]
Nanorods	10	Di Stasio et al. [114]
Nanoplatelets	2.49	Guzelturk et al. [108]

7 Conclusion and future outlook

Colloidal semiconductor materials offer high efficiencies for lighting applications and their narrow emission spectrum allows for fine-tuning of the generated white-light spectrum. With these materials, high color rendition performance, large overlap with the human eye sensitivity function and warm-white shade can be realized at the same time. The recent emergence of narrower emitters such as NPLs makes the color control even better. There is still room for the development of high-efficiency white LEDs using this new class of emitters. When electroluminescent LEDs are considered, the stability of these colloidal materials needs to be improved so that devices can reliably work under high-current operations. This of course involves a careful band-alignment engineering of the whole electroluminescent device. In addition, efficient green-emitting and blue-emitting devices have to be fabricated so that low power operation targets can be realized. Finally, despite the fact that internal quantum efficiency of the red-emitting colloidal LEDs hits almost unity, outcoupling of the light still needs to be improved. By involving light-extraction features, the EQEs of the devices can be substantially increased.

On the other hand, the utilization of colloidal materials in displays has already found use in industry, thanks to the narrow emission of high-efficiency QDs enabling displays with purer colors. With these materials, significantly broad color gamuts beyond the requirements of NTSC were realized. However, further improvements in these devices could still be possible if high-efficiency narrow emitters such as NPLs and some narrow band-emitting perovskites could be employed. The main bottlenecks for this approach, however, are the low stability and low quantum efficiencies of these materials in solid films. Another important problem that needs to be addressed for the displays based on liquid crystals is the energy loss due to polarizers. The realization of efficient emitters that inherently emit polarized light can significantly improve the efficiency of displays.

The colloidal materials offer convenient flexibility in terms of choosing the lasing wavelength in the visible and infrared; however, to reach the ultimate goal of their electroluminescent lasers requires overcoming serious problems of colloidal materials including suppression of loss mechanisms and increasing stability of the emitter materials. To date optically excited lasers of QDs, nanorods, NPLs, and perovskites were successfully demonstrated with pump lasers of femtosecond pulse widths. Nevertheless, lasing in continuous pumping regime in a robust manner is still problematic. The utilization of high-absorption cross section materials such as NPLs seems to be promising, but further improvements are still needed.

Considering the developments witnessed in the past decades, we believe that the practical problems associated with the use of colloidal materials in LEDs, displays, and lasers will be overcome in the near future. Within the last 15 years, the efficiency of the colloidal QDs have risen from a few percent to almost unity, their stabilities were significantly improved, and they were successfully employed in LEDs, displays, and lasers. With the developments in the synthesis and composition, structure and shape control of colloidal materials, they have a great potential to overcome current difficulties and enter the commercialization phase in various applications.

Acknowledgement: The authors acknowledge ESF EURYI, EU-FP7 Nanophotonics4Energy NoE, and TUBITAK EEEAG 110E217, 112E183, 114F326, and 114E449, and in part by NRF-CRP-6-2010-02 and NRF-RF-2009-09. H.V.D. acknowledges additional support from TUBA-GEBIP and T.E. acknowledges support from TUBITAK BIDEB.

References

[1] Lu, Z.; Yin, Y. Colloidal Nanoparticle Clusters: Functional Materials by Design. *Chem. Soc. Rev.***2012**, *41* (21), 6874–6887.

[2] Shirasaki, Y.; Supran, G. J.; Bawendi, M. G.; Bulović, V. Emergence of Colloidal Quantum-Dot Light-Emitting Technologies. *Nat. Photonics***2013**, *7* (12), 933–933.

[3] Velegol, D. Assembling Colloidal Devices by Controlling Interparticle Forces. *J. Nanophotonics***2007**, *1* (1), 012502.

[4] Furumi, S.; Fudouzi, H.; Sawada, T. Self-Organized Colloidal Crystals for Photonics and Laser Applications. *Laser Photonics Rev.***2010**, *4* (2), 205–220.

[5] Sargent, E. H. Colloidal Quantum Dot Solar Cells. *Nat. Photonics***2012**, *6* (3), 133–135.

[6] Kim, S.-H.; Lee, S. Y.; Yang, S.-M.; Yi, G.-R. Self-Assembled Colloidal Structures for Photonics. *NPG Asia Mater.***2011**, *3* (1), 25–33.

[7] Sappala, T. J. Samsung's high-end TVs use nanocrystals for better color, efficiency http://www.engadget.com/2015/01/05/ces2015-samsung-suhd/ (accessed Dec 11, 2015).

[8] Nanosys. Welcome to a revolution in color http://www.nanosysinc.com/lcd-revolution/ (accessed Dec 11, 2015).

[9] Kim, J. Y.; Voznyy, O.; Zhitomirsky, D.; Sargent, E. H. Colloidal Quantum Dot Materials and Devices: A Quarter-Century of Advances. *Adv. Mater.***2013**, *25* (36), 4986–5010.

[10] Nizamoglu, S.; Erdem, T.; Wei Sun, X.; Volkan Demir, H. Warm-White Light-Emitting Diodes Integrated with Colloidal Quantum Dots for High Luminous Efficacy and Color Rendering: Reply to Comment. *Opt. Lett.***2011**, *36* (15), 2852.

[11] Erdem, T.; Kelestemur, Y.; Soran-Erdem, Z.; Ji, Y.; Demir, H. V. Energy-Saving Quality Road Lighting with Colloidal Quantum Dot Nanophosphors. *Nanophotonics***2014**, *3* (6).

[12] Erdem, T.; Nizamoglu, S.; Sun, X. W.; Demir, H. V. A Photometric Investigation of Ultra-Efficient LEDs with High Color Rendering Index and High Luminous Efficacy Employing Nanocrystal Quantum Dot Luminophores. *Opt. Express***2010**, *18* (1), 340–347.

[13] Graydon, O. The New Oil? *Nat. Photonics***2011**, *5* (1), 1.

[14] Erdem, T.; Demir, H. V. Semiconductor Nanocrystals as Rare-Earth Alternatives. *Nat. Photonics***2011**, *5* (1), 126.

[15] Erdem, T.; Demir, H. V. Color Science of Nanocrystal Quantum Dots for Lighting and Displays. *Nanophotonics***2013**, *2* (1), 57–81.

[16] Luo, Z.; Xu, D.; Wu, S.; Paper, I. Emerging Quantum-Dots-Enhanced LCDs. *J. Disp. Technol.***2014**, *10* (7), 526–539.

[17] Klimov, V. I.; Mikhailovsky, A. A.; Xu, S.; Malko, A.; Hollingsworth, J. A.; Leatherdale, C. A.; Eisler, H.-J.; Bawendi, M. G. Optical Gain and Stimulated Emission in Nanocrystal Quantum Dots. *Science (80-.).***2000**, *290* (5490), 314–317.

[18] Whitaker, T. Osram Opto demonstrates 142 lm/W warm-white LED http://www.ledsmagazine.com/articles/2011/03/osram-opto-demonstrates-142-lm-w-warm-white-led.html (accessed Dec 11, 2015).

[19] Kim, K.; Woo, J. Y.; Jeong, S.; Han, C. S. Photoenhancement of a Quantum Dot Nanocomposite via Uv Annealing and Its Application to White LEDs. *Adv. Mater.***2011**, *23* (7), 911–914.

[20] Liang, R.; Yan, D.; Tian, R.; Yu, X.; Shi, W.; Li, C.; Wei, M.; Evans, D. G.; Duan, X. Quantum Dots-Based Flexible Films and Their Application as the Phosphor in White Light-Emitting Diodes. *Chem. Mater.***2014**, *26* (8), 2595–2600.

[21] Erdem, T.; Nizamoglu, S.; Demir, H. V. Computational Study of Power Conversion and Luminous Efficiency Performance for Semiconductor Quantum Dot Nanophosphors on Light-Emitting Diodes. *Opt. Express***2012**, *20* (3), 3275–3295.

[22] Zhao, B.; Zhang, D.; Sun, K.; Wang, X.; Mao, R.; Li, W. Intrinsic Quantum Dot Based White-Light-Emitting Diodes with a Layered Coating Structure for Reduced Reabsorption of Multiphase Phosphors. *RSC Adv.***2014**, *4* (85), 45155–45158.

[23] Zhang, Z.; Luan, S.; Huang, K.; Zhang, Y.; Shi, Z.; Xie, R.; Yang, W. Single-Phase Dual Emissive Cu:CdS–ZnSe Core–shell Nanocrystals with "zero Self-Absorption" and Their Application in White Light Emitting Diodes. *J. Mater. Chem. C***2015**, *3* (15), 3614–3622.

[24] Xuan, T.-T.; Liu, J.-Q.; Xie, R.-J.; Li, H.-L.; Sun, Z. Microwave-Assisted Synthesis of CdS/ZnS:Cu Quantum Dots for White Light-Emitting Diodes with High Color Rendition. *Chem. Mater.***2015**, *27* (4), 1187–1193.

[25] Zhao, Y.; Riemersma, C.; Pietra, F.; Koole, R.; de Mello Donega, C.; Meijerink, a. High-Temperature Luminescence Quenching of Colloidal Quantum Dots. *ACS Nano***2012**, *6* (10), 9058–9067.

[26] Jun, S.; Lee, J.; Jang, E. Highly Luminescent and Photostable Quantum Dot-Silica Monolith and Its Application to Light-Emitting Diodes. *ACS Nano***2013**, *7* (2), 1472–1477.

[27] Alejandro-Arellano, M.; Ung, T.; Blanco, Á.; Mulvaney, P.; Liz-Marzán, L. M. Silica-Coated Metals and Semiconductors. Stabilization and Nanostructuring. *Pure Appl. Chem.***2000**, *72* (1-2), 257–267.

[28] Yoo, H.; Jang, H. S.; Lee, K.; Woo, K. Quantum Dot-Layer-Encapsulated and Phenyl-Functionalized Silica Spheres for Highly Luminous, Colour Rendering, and Stable White Light-Emitting Diodes. *Nanoscale***2015**, *7* (30), 12860–12867.

[29] Otto, T.; Müller, M.; Mundra, P.; Lesnyak, V.; Demir, H. V.; Gaponik, N.; Eychmüller, A. Colloidal Nanocrystals Embedded in Macrocrystals: Robustness, Photostability, and Color Purity. *Nano Lett.***2012**, *12* (10), 5348–5354.

[30] Erdem, T.; Soran-Erdem, Z.; Hernandez-Martinez, P. L.; Sharma, V. K.; Akcali, H.; Akcali, I.; Gaponik, N.; Eychmüller, A.; Demir, H. V. Sweet Plasmonics: Sucrose Macrocrystals of Metal Nanoparticles. *Nano Res.***2014**, *8* (3), 860–869.

[31] Yuan, X.; Ma, R.; Zhang, W.; Hua, J.; Meng, X.; Zhong, X.; Zhang, J.; Zhao, J.; Li, H. Dual Emissive Manganese and Copper Co-Doped Zn–In–S Quantum Dots as a Single Color-Converter for High Color Rendering White-Light-Emitting Diodes. *ACS Appl. Mater. Interfaces***2015**, *7*, 8659–8666.

[32] Dang, C.; Lee, J.; Zhang, Y.; Han, J.; Breen, C.; Steckel, J. S.; Coe-Sullivan, S.; Nurmikko, A. A Wafer-Level Integrated White-Light-Emitting Diode Incorporating Colloidal Quantum Dots as a Nanocomposite Luminescent Material. *Adv. Mater.***2012**, *24* (44), 5915–5918.

[33] Kalytchuk, S.; Zhovtiuk, O.; Rogach, A. L. Sodium Chloride Protected CdTe Quantum Dot Based Solid-State Luminophores with High Color Quality and Fluorescence Efficiency. *Appl. Phys. Lett.***2013**, *103* (10), 103105.

[34] Müller, M.; Kaiser, M.; Stachowski, G. M.; Resch-Genger, U.; Gaponik, N.; Eychmüller, A. Photoluminescence Quantum Yield and Matrix-Induced Luminescence Enhancement of Colloidal Quantum Dots Embedded in Ionic Crystals. *Chem. Mater.***2014**, *26* (10), 3231–3237.

[35] Erdem, T.; Soran-Erdem, Z.; Sharma, V. K.; Kelestemur, Y.; Adam, M.; Gaponik, N.; Demir, H. V. Stable and Efficient Colour Enrichment Powders of Nonpolar Nanocrystals in LiCl. *Nanoscale***2015**, *7* (42), 17611–17616.

[36] Ye, L.; Yong, K.-T.; Liu, L.; Roy, I.; Hu, R.; Zhu, J.; Cai, H.; Law, W.-C.; Liu, J.; Wang, K.; et al. A Pilot Study in Non-Human Primates Shows No Adverse Response to Intravenous Injection of Quantum Dots. *Nat. Nanotechnol.***2012**, *7* (7), 453–458.

[37] Chen, B.; Zhou, Q.; Li, J.; Zhang, F.; Liu, R.; Zou, B. Red Emissive CuInS2 -Based Nanocrystals: A Potential Phosphor for Warm White Light- Emitting Diodes. *Opt. Express***2013**, *21* (8), 10105–10110.

[38] Chen, B.; Zhong, H.; Wang, M.; Liu, R.; Zou, B. Integration of CuInS2-Based Nanocrystals for High Efficiency and High Colour Rendering White Light-Emitting Diodes. *Nanoscale***2013**, *5* (8), 3514–3519.

[39] Kim, J.-H.; Yang, H. White Lighting Device from Composite Films Embedded with Hydrophilic Cu(In, Ga)S2/ZnS and Hydrophobic InP/ZnS Quantum Dots. *Nanotechnology***2014**, *25* (22), 225601.

[40] Yoon, H. C.; Oh, J. H.; Ko, M.; Yoo, H.; Do, Y. R. Synthesis and Characterization of Green Zn-Ag-In-S and Red Zn-Cu-In-S Quantum Dots for Ultrahigh Color Quality of down-Converted White LEDs. *ACS Appl. Mater. Interfaces***2015**, *7* (13), 7342–7350.

[41] Huang, B.; Dai, Q.; Zhuo, N.; Jiang, Q.; Shi, F.; Wang, H.; Zhang, H.; Liao, C.; Cui, Y.; Zhang, J. Bicolor Mn-Doped CuInS2/ZnS Core/shell Nanocrystals for White Light-Emitting Diode with High Color Rendering Index. *J. Appl. Phys.***2014**, *116* (9), 094303.

[42] Yuan, X.; Hua, J.; Zeng, R.; Zhu, D.; Ji, W.; Jing, P.; Meng, X.; Zhao, J.; Li, H. Efficient White Light Emitting Diodes Based on Cu-Doped ZnInS/ZnS Core/shell Quantum Dots. *Nanotechnology***2014**, *25* (43), 435202.

[43] Zhang, Z.; Liu, D.; Li, D.; Huang, K.; Zhang, Y.; Shi, Z.; Xie, R.; Han, M.-Y.; Wang, Y.; Yang, W. Dual Emissive Cu:InP/ZnS/InP/ZnS Nanocrystals: Single-Source "Greener" Emitters with Flexibly Tunable Emission from Visible to Near-Infrared and Their Application in White Light-Emitting Diodes. *Chem. Mater.***2015**, *27* (4), 1405–1411.

[44] Shang, C.; Shang, X.; Qu, Y.; Li, M. Investigation on the Red Shift of Charge Transfer Excitation Spectra for Nano-Sized Y2O3:Eu3+. *Chem. Phys. Lett.***2011**, *501* (4-6), 480–484.

[45] Dai, Q.; Foley, M.; Breshike, C. Ligand-Passivated Eu: Y2O3 Nanocrystals as a Phosphor for White Light Emitting Diodes. *J. Am. Chem. Soc.***2011**, *133* (39), 15475–15486.

[46] Lü, Y.; Tang, X.; Yan, L.; Li, K.; Liu, X.; Shang, M.; Li, C.; Lin, J. Synthesis and Luminescent Properties of GdNbO 4?:RE 3+ (RE = Tm, Dy) Nanocrystalline Phosphors via the Sol–Gel Process. *J. Phys. Chem. C***2013**, *117* (42), 21972–21980.

[47] Wang, T.; Li, P.; Li, H. Color-Tunable Luminescence of Organoclay-Based Hybrid Materials Showing Potential Applications in White LED and Thermosensors. *ACS Appl. Mater. Interfaces***2014**, *6* (15), 12915–12921.

[48] Bai, X.; Caputo, G.; Hao, Z.; Freitas, V. T.; Zhang, J.; Longo, R. L.; Malta, O. L.; Ferreira, R. A. S.; Pinna, N. Efficient and Tuneable Photoluminescent Boehmite Hybrid Nanoplates Lacking Metal Activator Centres for Single-Phase White LEDs. *Nat. Commun.***2014**, *5*, 5702.

[49] Koo, W. H.; Jeong, S. M.; Araoka, F.; Ishikawa, K.; Nishimura, S.; Toyooka, T.; Takezoe, H. Light Extraction from Organic Light-Emitting Diodes Enhanced by Spontaneously Formed Buckles. *Nat. Photonics***2010**, *4* (4), 222–226.

[50] Kim, J. B.; Lee, J. H.; Moon, C. K.; Kim, S. Y.; Kim, J. J. Highly Enhanced Light Extraction from Surface Plasmonic Loss Minimized Organic Light-Emitting Diodes. *Adv. Mater.***2013**, *25* (26), 3571–3577.

[51] Peng, H. J.; Ho, Y. L.; Yu, X. J.; Kwok, H. S. Enhanced Coupling of Light from Organic Light Emitting Diodes Using Nanoporous Films. *J. Appl. Phys.***2004**, *96* (3), 1649–1654.

[52] Matioli, E.; Weisbuch, C. Impact of Photonic Crystals on LED Light Extraction Efficiency: Approaches and Limits to Vertical Structure Designs. *J. Phys. D. Appl. Phys.***2010**, *43* (35), 354005.

[53] Lin, C. F.; Yang, Z. J.; Zheng, J. H.; Dai, J. J. Enhanced Light Output in Nitride-Based Light-Emitting Diodes by Roughening the Mesa Sidewall. *IEEE Photonics Technol. Lett.***2005**, *17* (10), 2038–2040.

[54] Truong, T. A.; Campos, L. M.; Matioli, E.; Meinel, I.; Hawker, C. J.; Weisbuch, C.; Petroff, P. M. Light Extraction from GaN-Based Light Emitting Diode Structures with a Noninvasive Two-Dimensional Photonic Crystal. *Appl. Phys. Lett.***2009**, *94* (2), 023101.

[55] Kim, T. S.; Kim, S. M.; Jang, Y. H.; Jung, G. Y. Increase of Light Extraction from GaN Based Light Emitting Diodes Incorporating Patterned Structure by Colloidal Lithography. *Appl. Phys. Lett.***2007**, *91* (17), 171114.

[56] Diana, F. S.; David, A.; Meinel, I.; Sharma, R.; Weisbuch, C.; Nakamura, S.; Petroff, P. M. Photonic Crystal-Assisted Light Extraction from a Colloidal Quantum Dot/GaN Hybrid Structure. *Nano Lett.***2006**, *6* (6), 1116–1120.

[57] Yang, X.; Dev, K.; Wang, J.; Mutlugun, E.; Dang, C.; Zhao, Y.; Liu, S.; Tang, Y.; Tan, S. T.; Sun, X. W.; et al. Light Extraction Efficiency Enhancement of Colloidal Quantum Dot Light-Emitting Diodes Using Large-Scale Nanopillar Arrays. *Adv. Funct. Mater.***2014**, *24* (38), 5977–5984.

[58] Zhu, R.; Luo, Z.; Wu, S.-T. Light Extraction Analysis and Enhancement in a Quantum Dot Light Emitting Diode. *Opt. Express***2014**, *22* (S7), A1783–A1798.

[59] Liang, H.; Zhu, R.; Dong, Y.; Wu, S.-T.; Li, J.; Wang, J.; Zhou, J. Enhancing the Outcoupling Efficiency of Quantum Dot LEDs with Internal Nano-Scattering Pattern. *Opt. Express***2015**, *23* (10), 12910–12922.

[60] Hu, R.; Fu, X.; Zou, Y.; Luo, X. A Complementary Study to "toward Scatter-Free Phosphors in White Phosphor-Converted Light-Emitting Diodes:" Comment. *Opt. Express***2013**, *21* (4), 5071–5073.

[61] Fang, C. Y.; Liu, Y. L.; Lee, Y. C.; Chen, H. L.; Wan, D. H.; Yu, C. C. Nanoparticle Stacks with Graded Refractive Indices Enhance the Omnidirectional Light Harvesting of Solar Cells and the Light Extraction of Light-Emitting Diodes. *Adv. Funct. Mater.***2013**, *23* (11), 1412–1421.

[62] Colvin, V. L.; Schlamp, M. C.; Alivisatos, a P. Light-Emitting-Diodes Made from Cadmium Selenide Nanocrystals and a Semiconducting Polymer. *Nature***1994**, *370* (6488), 354–357.

[63] Dai, X.; Zhang, Z.; Jin, Y.; Niu, Y.; Cao, H.; Liang, X.; Chen, L.; Wang, J.; Peng, X. Solution-Processed, High-Performance Light-Emitting Diodes Based on Quantum Dots. *Nature***2014**, *515* (7525), 96–99.

[64] Anikeeva, P. O.; Halpert, J. E.; Bawendi, M. G.; Bulović, V. Quantum Dot Light-Emitting Devices with Electroluminescence Tunable over the Entire Visible Spectrum. *Nano Lett.***2009**, *9* (7),

2532–2536.

[65] Bae, W. K.; Park, Y.-S.; Lim, J.; Lee, D.; Padilha, L. a; McDaniel, H.; Robel, I.; Lee, C.; Pietryga, J. M.; Klimov, V. I. Controlling the Influence of Auger Recombination on the Performance of Quantum-Dot Light-Emitting Diodes. *Nat. Commun.***2013**, *4*, 2661.

[66] Mashford, B.; Stevenson, M.; Popovic, Z. High-Efficiency Quantum-Dot Light-Emitting Devices with Enhanced Charge Injection. *Nat. Photonics***2013**, *7* (4), 407–412.

[67] Lim, J.; Park, M.; Bae, W. K.; Lee, D.; Lee, S.; Lee, C.; Char, K. Highly Efficient Cadmium-Free Quantum Dot Light-Emitting Diodes Enabled by the Direct Formation of Excitons within InP@ZnSeS Quantum Dots. *ACS Nano***2013**, *7* (10), 9019–9026.

[68] Wang, J.; Wang, N.; Jin, Y.; Si, J.; Tan, Z.-K.; Du, H.; Cheng, L.; Dai, X.; Bai, S.; He, H.; et al. Interfacial Control Toward Efficient and Low-Voltage Perovskite Light-Emitting Diodes. *Adv. Mater.***2015**, *27* (14), 2311–2316.

[69] Coe, S.; Woo, W.-K.; Bawendi, M.; Bulovic, V. Electroluminescence from Single Monolayers of Nanocrystals in Molecular Organic Devices. *Nature***2002**, *420* (6917), 800–803.

[70] Coe-Sullivan, S.; Steckel, J. S.; Woo, W. K.; Bawendi, M. G.; Bulovic, V. Large-Area Ordered Quantum-Dot Monolayers via Phase Separation during Spin-Casting. *Adv. Funct. Mater.***2005**, *15* (7), 1117–1124.

[71] Anikeeva, P. O.; Halpert, J. E.; Bawendi, M. G.; Bulović, V. Electroluminescence from a Mixed Red-Green-Blue Colloidal Quantum Dot Monolayer. *Nano Lett.***2007**, *7* (8), 2196–2200.

[72] Caruge, J. M.; Halpert, J. E.; Wood, V.; Bulović, V.; Bawendi, M. G. Colloidal Quantum-Dot Light-Emitting Diodes with Metal-Oxide Charge Transport Layers. *Nat. Photonics***2008**, *2* (4), 247–250.

[73] Woo, W. K.; Shimizu, K. T.; Jarosz, M. V.; Neuhauser, R. G.; Leatherdale, C. A.; Rubner, M. A.; Bawendi, M. G. Reversible Charging of CdSe Nanocrystals in a Simple Solid-State Device. *Adv. Mater.***2002**, *14* (15), 1068–1071.

[74] Galland, C.; Ghosh, Y.; Steinbrück, A.; Sykora, M.; Hollingsworth, J. A.; Klimov, V. I.; Htoon, H. Two Types of Luminescence Blinking Revealed by Spectroelectrochemistry of Single Quantum Dots. *Nature***2011**, *479* (7372), 203–207.

[75] Dong, Y.; Caruge, J.-M.; Zhou, Z.; Hamilton, C.; Popovic, Z.; Ho, J.; Stevenson, M.; Liu, G.; Bulovic, V.; Bawendi, M.; et al. Ultra-Bright, Highly Efficient, Low Roll-Off Inverted Quantum-Dot Light Emitting Devices (QLEDs). *SID Symp. Dig. Tech. Pap.***2015**, *46* (1), 270–273.

[76] Lim, J.; Bae, W. K.; Lee, D.; Nam, M. K.; Jung, J.; Lee, C.; Char, K.; Lee, S. InP@ZnSeS, Core@composition Gradient Shell Quantum Dots with Enhanced Stability. *Chem. Mater.***2011**, *23* (20), 4459–4463.

[77] Yang, X.; Zhao, D.; Leck, K. S.; Tan, S. T.; Tang, Y. X.; Zhao, J.; Demir, H. V.; Sun, X. W. Full Visible Range Covering InP/ZnS Nanocrystals with High Photometric Performance and Their Application to White Quantum Dot Light-Emitting Diodes. *Adv. Mater.***2012**, *24* (30), 4180–4185.

[78] Tan, Z.-K.; Moghaddam, R. S.; Lai, M. L.; Docampo, P.; Higler, R.; Deschler, F.; Price, M.; Sadhanala, A.; Pazos, L. M.; Credgington, D.; et al. Bright Light-Emitting Diodes Based on Organometal Halide Perovskite. *Nat. Nanotechnol.***2014**, *9*, 687–692.

[79] Kim, Y.-H.; Cho, H.; Heo, J. H.; Kim, T.-S.; Myoung, N.; Lee, C.-L.; Im, S. H.; Lee, T.-W. Multicolored Organic/Inorganic Hybrid Perovskite Light-Emitting Diodes. *Adv. Mater.***2015**, *27* (7), 1248–1254.

[80] Jaramillo-Quintero, O. a.; Sánchez, R. S.; Rincón, M.; Mora-Sero, I. Bright Visible-Infrared Light Emitting Diodes Based on Hybrid Halide Perovskite with Spiro-OMeTAD as a Hole Injecting Layer. *J. Phys. Chem. Lett.***2015**, *6* (10), 1883–1890.

[81] Li, G.; Tan, Z.-K.; Di, D.; Lai, M. L.; Jiang, L.; Lim, J. H.; Friend, R. H.; Greenham, N. C. Efficient Light-Emitting Diodes Based on Nano-Crystalline Perovskite in a Dielectric Polymer Matrix. *Nano Lett.***2015**, *15* (4), 2640–2644.

[82] Chen, Z.; Nadal, B.; Mahler, B.; Aubin, H.; Dubertret, B. Quasi-2D Colloidal Semiconductor Nanoplatelets for Narrow Electroluminescence. *Adv. Funct. Mater.***2014**, *24* (3), 295–302.

[83] Vitukhnovsky, A. G.; Lebedev, V. S.; Selyukov, A. S.; Vashchenko, A. A.; Vasiliev, R. B.; Sokolikova, M. S. Electroluminescence from Colloidal Semiconductor CdSe Nanoplatelets in Hybrid Organic–inorganic Light Emitting Diode. *Chem. Phys. Lett.***2015**, *619*, 185–188.

[84] Fan, F.; Kanjanaboos, P.; Saravanapavanantham, M.; Beauregard, E.; Ingram, G.; Yassitepe, E.; Adachi, M. M.; Voznyy, O.; Johnston, A. K.; Walters, G.; et al. Colloidal CdSe 1– X S X Nanoplatelets with Narrow and Continuously-Tunable Electroluminescence. *Nano Lett.***2015**, *15* (7), 4611–4615.

[85] Jang, E.; Jun, S.; Jang, H.; Lim, J.; Kim, B.; Kim, Y. White-Light-Emitting Diodes with Quantum Dot Color Converters for Display Backlights. *Adv. Mater.***2010**, *22* (28), 3076–3080.

[86] Chen, K.-J.; Chen, H.-C.; Tsai, K.-A.; Lin, C.-C.; Tsai, H.-H.; Chien, S.-H.; Cheng, B.-S.; Hsu, Y.-J.; Shih, M.-H.; Tsai, C.-H.; et al. Resonant-Enhanced Full-Color Emission of Quantum-Dot-Based Display Technology Using a Pulsed Spray Method. *Adv. Funct. Mater.***2012**, *22* (24), 5138–5143.

[87] Luo, Z.; Chen, Y.; Wu, S.-T. Wide Color Gamut LCD with a Quantum Dot Backlight. *Opt. Express***2013**, *21* (22), 26269–26284.

[88] Zhang, F.; Zhong, H.; Chen, C.; Wu, X.; Hu, X.; Huang, H. Brightly Luminescent and Color- (X = Br, I, Cl) Quantum Dots?: Potential Alternatives for Display Technology. *ACS Nano***2015**, *3* (4), 4533–4542.

[89] Protesescu, L.; Yakunin, S.; Bodnarchuk, M. I.; Krieg, F.; Caputo, R.; Hendon, C. H.; Yang, R. X.; Walsh, A.; Kovalenko, M. V. Nanocrystals of Cesium Lead Halide Perovskites (CsPbX 3, X = Cl, Br, and I): Novel Optoelectronic Materials Showing Bright Emission with Wide Color Gamut. *Nano Lett.***2015**, *15* (6), 3692–3696.

[90] Kim, L.; Anikeeva, P. O.; Coe-Sullivan, S. a.; Steckel, J. S.; Bawendi, M. G.; Bulović, V. Contact Printing of Quantum Dot Light-Emitting Devices. *Nano Lett.***2008**, *8* (12), 4513–4517.

[91] Kim, T.-H.; Cho, K.-S.; Lee, E. K.; Lee, S. J.; Chae, J.; Kim, J. W.; Kim, D. H.; Kwon, J.-Y.; Amaratunga, G.; Lee, S. Y.; et al. Full-Colour Quantum Dot Displays Fabricated by Transfer Printing. *Nat. Photonics***2011**, *5* (3), 176–182.

[92] Choi, M. K.; Yang, J.; Kang, K.; Kim, D. C.; Choi, C.; Park, C.; Kim, S. J.; Chae, S. I.; Kim, T.-H.; Kim, J. H.; et al. Wearable Red–green–blue Quantum Dot Light-Emitting Diode Array Using High-Resolution Intaglio Transfer Printing. *Nat. Commun.***2015**, *6*, 7149.

[93] Haverinen, H. M.; Myllyla, R. a.; Jabbour, G. E. Inkjet Printed RGB Quantum Dot-Hybrid LED. *J. Disp. Technol.***2010**, *6* (3), 87–89.

[94] Kong, Y. L.; Tamargo, I. a; Kim, H.; Johnson, B. N.; Gupta, M. K.; Koh, T.-W.; Chin, H.-A.; Steingart, D. a; Rand, B. P.; Mcalpine,

M. C. 3D Printed Quantum Dot Light-Emitting Diodes. *Nano Lett.***2014**, *14* (12), 7017–7023.

[95] Kim, B. H.; Onses, M. S.; Lim, J. Bin; Nam, S.; Oh, N.; Kim, H.; Yu, K. J.; Lee, J. W.; Kim, J.-H.; Kang, S.-K.; et al. High-Resolution Patterns of Quantum Dots Formed by Electrohydrodynamic Jet Printing for Light-Emitting Diodes. *Nano Lett.***2015**, *15* (2), 969–973.

[96] Bae, W. K.; Lim, J.; Lee, D.; Park, M.; Lee, H.; Kwak, J.; Char, K.; Lee, C.; Lee, S. R/G/B/Natural White Light Thin Colloidal Quantum Dot-Based Light-Emitting Devices. *Adv. Mater.***2014**, *26* (37), 6387–6393.

[97] Oh, J. H.; Lee, K.-H.; Yoon, H. C.; Yang, H.; Do, Y. R. Color-by-Blue Display Using Blue Quantum Dot Light-Emitting Diodes and Green/red Color Converting Phosphors. *Opt. Express***2014**, *22* (S2), A511–A520.

[98] Dang, C.; Lee, J.; Breen, C.; Steckel, J. S.; Coe-Sullivan, S.; Nurmikko, A. Red, Green and Blue Lasing Enabled by Single-Exciton Gain in Colloidal Quantum Dot Films. *Nat. Nanotechnol.***2012**, *7* (5), 335–339.

[99] Klimov, V. I. Quantization of Multiparticle Auger Rates in Semiconductor Quantum Dots. *Science***2000**, *287* (5455), 1011–1013.

[100] Eisler, H. J.; Sundar, V. C.; Bawendi, M. G.; Walsh, M.; Smith, H. I.; Klimov, V. Color-Selective Semiconductor Nanocrystal Laser. *Appl. Phys. Lett.***2002**, *80* (24), 4614–4616.

[101] Malko, A. V.; Mikhailovsky, A. A.; Petruska, M. A.; Hollingsworth, J. A.; Htoon, H.; Bawendi, M. G.; Klimov, V. I. From Amplified Spontaneous Emission to Microring Lasing Using Nanocrystal Quantum Dot Solids. *Appl. Phys. Lett.***2002**, *81* (7), 1303–1305.

[102] Chan, Y.; Steckel, J. S.; Snee, P. T.; Caruge, J. M.; Hodgkiss, J. M.; Nocera, D. G.; Bawendi, M. G. Blue Semiconductor Nanocrystal Laser. *Appl. Phys. Lett.***2005**, *86* (7), 073102.

[103] Zhang, C.; Zhang, F.; Cheng, A.; Kimball, B.; Wang, A. Y.; Xu, J. Frequency Upconverted Lasing of Nanocrystal Quantum Dots in Microbeads. *Appl. Phys. Lett.***2009**, *95* (18), 10–13.

[104] Dang, C.; Lee, J.; Roh, K.; Kim, H.; Ahn, S.; Jeon, H.; Breen, C.; Steckel, J. S.; Coe-Sullivan, S.; Nurmikko, a. Highly Efficient, Spatially Coherent Distributed Feedback Lasers from Dense Colloidal Quantum Dot Films. *Appl. Phys. Lett.***2013**, *103* (17), 8–13.

[105] Roh, K.; Dang, C.; Lee, J.; Chen, S.; Steckel, J. S.; Coe-Sullivan, S.; Nurmikko, A. Surface-Emitting Red, Green, and Blue Colloidal Quantum Dot Distributed Feedback Lasers. *Opt. Express***2014**, *22* (15), 18800–18806.

[106] Wang, Y.; Leck, K. S.; Ta, V. D.; Chen, R.; Nalla, V.; Gao, Y.; He, T.; Demir, H. V.; Sun, H. Blue Liquid Lasers from Solution of CdZnS/ZnS Ternary Alloy Quantum Dots with Quasi-Continuous Pumping. *Adv. Mater.***2015**, *27* (1), 169–175.

[107] Guzelturk, B.; Kelestemur, Y.; Gungor, K.; Yeltik, A.; Akgul, M. Z.; Wang, Y.; Chen, R.; Dang, C.; Sun, H.; Demir, H. V. Stable and Low-Threshold Optical Gain in CdSe/CdS Quantum Dots: An All-Colloidal Frequency Up-Converted Laser. *Adv. Mater.***2015**, *27* (17), 2741–2746.

[108] Guzelturk, B.; Kelestemur, Y.; Olutas, M.; Delikanli, S.; Demir, H. V. Amplified Spontaneous Emission and Lasing in Colloidal Nanoplatelets. *ACS Nano***2014**, *8* (7), 6599–6605.

[109] Deschler, F.; Price, M.; Pathak, S.; Klintberg, L. E.; Jarausch, D. D.; Higler, R.; Hüttner, S.; Leijtens, T.; Stranks, S. D.; Snaith, H. J.; et al. High Photoluminescence Efficiency and Optically Pumped Lasing in Solution-Processed Mixed Halide Perovskite Semiconductors. *J. Phys. Chem. Lett.***2014**, *5* (8), 1421–1426.

[110] Guzelturk, B.; Kelestemur, Y.; Akgul, M. Z.; Sharma, V. K.; Demir, H. V. Ultralow Threshold One-Photon- and Two-Photon-Pumped Optical Gain Media of Blue-Emitting Colloidal Quantum Dot Films. *J. Phys. Chem. Lett.***2014**, *5* (13), 2214–2218.

[111] Wang, Y.; Ta, V. D.; Gao, Y.; He, T. C.; Chen, R.; Mutlugun, E.; Demir, H. V.; Sun, H. D. Stimulated Emission and Lasing from CdSe/CdS/ZnS Core-Multi-Shell Quantum Dots by Simultaneous Three-Photon Absorption. *Adv. Mater.***2014**, *26* (18), 2954–2961.

[112] Xing, G.; Liao, Y.; Wu, X.; Chakrabortty, S.; Liu, X.; Yeow, E. K. L.; Chan, Y.; Sum, T. C. Ultralow-Threshold Two-Photon Pumped Amplified Spontaneous Emission and Lasing from Seeded CdSe/CdS Nanorod Heterostructures. *ACS Nano***2012**, *6* (12), 10835–10844.

[113] Gao, Y.; Ta, V. D.; Zhao, X.; Wang, Y.; Chen, R.; Mutlugun, E.; Fong, K. E.; Tan, S. T.; Dang, C.; Sun, X. W.; et al. Observation of Polarized Gain from Aligned Colloidal Nanorods. *Nanoscale***2015**, *7* (15), 6481–6486.

[114] Di Stasio, F.; Grim, J. Q.; Lesnyak, V.; Rastogi, P.; Manna, L.; Moreels, I.; Krahne, R. Single-Mode Lasing from Colloidal Water-Soluble CdSe/CdS Quantum Dot-in-Rods. *Small***2014**, *11* (11), 1328–1334.

[115] She, C.; Fedin, I.; Dolzhnikov, D. S.; Demortičre, A.; Schaller, R. D.; Pelton, M.; Talapin, D. V. Low-Threshold Stimulated Emission Using Colloidal Quantum Wells. *Nano Lett.***2014**, *14* (5), 2772–2777.

[116] García-Santamaría, F.; Chen, Y.; Vela, J.; Schaller, R. D.; Hollingsworth, J. A.; Klimov, V. I. Suppressed Auger Recombination in "Giant" Nanocrystals Boosts Optical Gain Performance. *Nano Lett.***2009**, *9* (10), 3482–3488.

[117] Olutas, M.; Guzelturk, B.; Kelestemur, Y.; Yeltik, A.; Delikanli, S.; Demir, H. V. Lateral Size-Dependent Spontaneous and Stimulated Emission Properties. *ACS Nano***2015**, *9* (5), 5041–5050.

[118] Grim, J. Q.; Christodoulou, S.; Di Stasio, F.; Krahne, R.; Cingolani, R.; Manna, L.; Moreels, I. Continuous-Wave Biexciton Lasing at Room Temperature Using Solution-Processed Quantum Wells. *Nat. Nanotechnol.***2014**, *9* (11), 891–895.

[119] Xing, G.; Mathews, N.; Lim, S. S.; Yantara, N.; Liu, X.; Sabba, D.; Grätzel, M.; Mhaisalkar, S.; Sum, T. C. Low-Temperature Solution-Processed Wavelength-Tunable Perovskites for Lasing. *Nat. Mater.***2014**, *13* (5), 476–480.

[120] Sutherland, B. R.; Hoogland, S.; Adachi, M. M.; Wong, C. T. O.; Sargent, E. H.; Al, S. E. T. Conformal Organohalide Perovskites Enable Lasing on Spherical Resonators. *ACS Nano***2014**, *8* (10), 10947–10952.